Research Square

Preprints are preliminary reports that have not undergone peer review.
They should not be considered conclusive, used to inform clinical practice,
or referenced by the media as validated information.

Adoptive NK cell transfer confers neuroprotection by attenuating neuroinflammation and alpha-synuclein pathology in a mouse model of synucleionpathy

Adetutu Adebowale
University of Georgia
Jung Ha Byun
University of Georgia
Jaegwon Chung
University of Georgia
Hyun Joon Lee
University of Georgia
Declan Gresham
University of Georgia
Jina Lim
University of Georgia
Jae-Kyung Lee
jamlee@uga.edu

University of Georgia

Research Article

Keywords: Parkinson's disease, NK cell, neuroinflammation, alpha-synuclein, Dopaminergic, Lewy pathology

Posted Date: August 14th, 2025

DOI: https://doi.org/10.21203/rs.3.rs-6558212/v1

License: This work is licensed under a Creative Commons Attribution 4.0 International License.
Read Full License

Additional Declarations: No competing interests reported.

Abstract

Background

Natural killer (NK) cells are key effector lymphoid cells involved in both innate and adaptive immunity and are capable of clearing abnormally aggregated α-synuclein (aSyn). In preclinical Parkinson's disease (PD) models, NK cell depletion worsens motor deficits and increases insoluble aSyn accumulation, suggesting a neuroprotective role. However, the therapeutic potential of NK cell transfer in modulating aSyn pathology and neurodegeneration remains unexplored.

Methods

To assess the efficacy of NK cell therapy, we administered biweekly systemic injection of untouched NK cells isolated from B6C3H donor mice into 2-month-old pre symptomatic homozygous M83 transgenic mice injected human aSyn preformed fibrils (PFFs). Neurological function was assessed via clasping behavior and clinical scoring. aSyn pathology and dopaminergic neurodegeneration were evaluated via immunohistochemistry. CyTOF-based immune profiling and multiplex ELISA were performed to characterize central and peripheral immune responses.

Results

Adoptive NK cell therapy improved motor function and reduced aSyn pathology in a region- and dose-dependent manner, with significant reductions in phosphorylated-aSyn (p-aSyn) and TH^+ neuronal loss in the substantia nigra. NK cell treatment modulated the CNS immune landscape by reducing $CD11b^+CD45^{high}$ and $MHCII^+$ activated microglial, $CD4^+$ T cells, and neutrophil infiltration, while promoting $CD19^+$ B and $CD8^+$ T cells. Similar immunomodulatory effects were observed in the periphery, including restoration of follicular B cells and reduced neutrophil frequencies. Mechanistically, aSyn exposure downregulated activating NK ligands and upregulated inhibitory receptor ligand mQa1b, along with p21 induction in microglia, suggesting a senescence-associated, immune-evasive phenotype that may contribute to reduced therapeutic efficacy at later disease stage.

Conclusions

Our study provides direct evidence of NK cells exerting neuroprotective and immunomodulatory effect in a preclinical model of synucleinopathy. These findings support NK cell transfer as a novel therapeutic strategy for PD and related neurodegenerative disorders.

BACKGROUND

Parkinson's disease (PD) is the second most common neurodegenerative disease after Alzheimer's disease (1). It is characterized by the aggregation of misfolded α-synuclein (aSyn), leading to Lewy body and Lewy neurite formation, as well as the progressive dopaminergic neurodegeneration in the substantia nigra pars compacta (SNpc) (2, 3) These pathological changes manifest as motor symptoms, including bradykinesia, tremor, rigidity and postural instability (4). While PD is primarily defined by its motor symptoms, non-motor symptoms such as cognitive decline, depression, gastrointestinal dysfunction, and sleep disturbances are increasingly recognized as major contributors to disease burden and reduced quality of life (5, 6).

Growing evidence suggests that neuroinflammation plays a critical role in PD progression. Elevated levels of pro-inflammatory cytokines including IL1β, IL2, IL6, IFNγ, and TNFα have been detected in the serum and cerebrospinal fluid (CSF) of PD patients (7), and correlates with disease severity (8). One potential driver of this inflammation is aSyn aggregation, which has been shown to hyperactivate microglia, leading to increased production of pro-inflammatory cytokines and reactive oxygen species, further exacerbating neuronal damage (9). The immune system plays a dual role in PD, contributing to both disease progression and potential neuroprotection. Clinical and preclinical studies have reported an increased proportion of $CD8^+$ T cells and a reduced in $CD4^+$ T cells in the peripheral blood of PD patients (10). Notably, $CD4^+$ T cell depletion protected mice from dopaminergic neurodegeneration in a mouse model of PD (11). Conversely, B cell depletion has been linked to greater dopaminergic neuron loss and worsened motor deficits, highlighting the complex role of adaptive immunity in PD (12).

NK cells are innate lymphocytes of growing interest in PD due to their dynamic roles in immune surveillance and emerging evidence of their involvement in neurodegenerative processes (13). NK cells are traditionally recognized as rapid responders capable of eliminating "missing-self" cells through cytotoxic mechanisms, and they play critical roles in antimicrobial defense (14, 15), clearance of senescent cells (16), regulation of inflammation (17, 18), and modulation of adaptive immune responses (19, 20). Recent transcriptomic studies have confirmed that NK cells reside within the brain under both homeostatic and pathological conditions (21, 22). In PD patients, NK cell numbers are higher in the blood and their activity level is associated with disease severity (23–25). In mice, in wild-type mice injected with α-syn PFF, NK cell frequency in the CNS increases compared to monomer-injected controls (26). Our previous work further demonstrated that systemic depletion of NK cells exacerbates disease pathology in the α-syn PFF M83 mouse model. NK cell-deficient mice exhibited significantly greater accumulation of α-syn pathology accompanied by elevated neuroinflammation (27), suggest a protective role for NK cells in limiting both α-syn burden and inflammatory activation during synucleinopathy. Building on these findings, the current study investigates whether adoptive NK cell transfer can therapeutically modulate disease progression, reduce neuropathology, and restore immune balance in the M83 α-synucleinopathy model.

We previously demonstrated that systemic NK cell depletion in a preclinical PD mouse model exacerbated aSyn pathology in the striatum, SNpc, and brainstem, increased neuroinflammation and worsened motor deficits (28), supporting a protective role of NK cells in PD. These findings suggested

that NK cells modulate neuroinflammation and facilitate the clearance of pathological protein aggregates (28). However, it remains unclear whether NK cell enrichment can mitigate motor deficits and reduce aSyn pathology. To address this, we employed the preformed fibril (PFF)-aSyn-injected M83 transgenic (Tg) mouse model, which recapitulates key features of α-synucleinopathies, including aggregate propagation and motor deficits. Using this model, we investigated whether systemic enrichment of NK cells modulates motor impairments and aSyn pathology. We assessed behavioral outcomes, synuclein burden, neurodegeneration, and neuroinflammatory responses, including immune cell profiling in the CNS and periphery using mass cytometry. NK cell infusion resulted in dose-dependent improvements in motor performance and reductions in neuroinflammation. These effects were accompanied by decreased aSyn accumulation in key brain regions, suggesting a potential modulatory role for NK cells in the progression of synucleinopathy. Together, these findings provide important insights into the therapeutic potential of NK cell-based interventions in Parkinson's disease.

METHODS

Mice

We used male and female M83 Tg mice (B6;C3-Tg(Prnp-SNCA*A53T)83Vle/J, homozygous, #004479 Jackson Laboratories) and B6C3F1/J mice (#100010 Jackson Laboratories). Mice were maintained in a climate-controlled facility with a 12-hour light/dark cycle. All research was performed in accordance with the NIH Guidelines for Animal Care and Use and approved by the Institutional Animal Care and Use Committee at The University of Georgia.

Recombinant aSyn and fibril preparation

Recombinant aSyn and fibrils were preparedas previously described (28). Recombinant human aSyn was expressed in E. coli BL21(DE3)/RIL cells and purified to >98% purity using size exclusion chromatography followed by Mono Q ion exchange chromatography, and further processed with high S cation exchange chromatography to reduce endotoxin, as previously described (29, 30). Final endotoxin levels were confirmed to be below 0.5 EU/mg. To validate the absence of biologically active endotoxin, a QUANTI-Blue™ assay was performed to assess TLR4-mediated NF-κB activation using HEK-Blue™ TLR4 reporter cells. For fibril formation, purified aSyn monomers were incubated at 37 °C at a concentration of 5 mg/mL with constant shaking (1100 rpm) for 7 days. Prior to surgical injection or in vitro application, fibrils were sonicated using a high-intensity Cup Horn sonicator (Qsonica Q700, 30% amplitude for 30 min). Fibril morphology and seed size were verified by transmission electron microscopy (TEM) as previously published (28).

Stereotaxic Surgery

Homozygous M83 Tg mice (8-week-old, male and female) were anesthetized with ketamine/xylazine (100 mg/kg and 10 mg/kg) and placed in a stereotaxic frame (KOPF) equipped with ear bars. Using sterile technique, animals received a unilateral intrastriatal injection of either human aSyn PFF or

monomeric aSyn (5 µg in 1 µL) into the right striatum. Stereotaxic coordinates relative to bregma were: anterior-posterior (AP) +0.3 mm, medial-lateral (ML) +2.3 mm, and dorsal-ventral (DV) −3.5 mm from the dural surface. Injections were delivered at a rate of 0.2 µL/min using a 29-gauge Hamilton syringe. Postoperatively and for the following 3 days, animals received subcutaneous injections of analgesics and were monitored meticulously for signs of pain and discomfort.

NK cell Isolation and Flow Cytometry

Following anesthesia with isoflurane, spleens were harvested from donor mice and processed to isolate splenocytes. Spleens were mechanically minced and suspended in cold PBS. After centrifugation at 1500 rpm for 10 minutes at room temperature, red blood cells were lysed using ACK lysing buffer (Quality Biological, Catalog# 118-156-101). Following lysis, cells were washed once with PBS, counted, and resuspended in PBS containing 2% fetal bovine serum (FBS). NK cells were then isolated using the EasySep™ Mouse NK Cell Isolation Kit (Stemcell Technologies, Catalog# 19855) following the manufacturer's protocol. The resulting enriched NK cell population—negatively selected and untouched—was resuspended in sterile 0.9% sodium chloride (normal saline) for injection. NK cells were injected to recipient mice via intraperitoneal (i.p.) injection. To evaluate the purity and subset distribution of isolated NK cells, splenocytes or isolated NK cells were resuspended in FACS buffer and stained for 30 minutes at 4 °C with TruStain FcX™ anti-mouse CD16/32 antibody (BioLegend, Cat# 101319) to block Fc receptors. Cells were subsequently incubated with fluorophore-conjugated antibodies against NK1.1 (Cat# 156514), CD45 (Cat# 109827), CD3 (Cat# 100241), CD19 (Cat# 115512), and CD11b (Cat# 101208), all from BioLegend. Following staining, cells were washed twice in 200 µL of FACS buffer and analyzed using the Novocyte Quanteon flow cytometer. Data were analyzed using FlowJo™ software (BD Biosciences).

Behavior assessment

To assess motor performance and disease progression, hind limb clasping behavior was evaluated in accordance with previously published protocols (31). Mice were gently suspended by the base of the tail, and the position of the hind limbs was observed over a 30-second period. Mice were tested every other week. Each session included three independent trials spaced one hour apart, and the average score across the three trials was recorded as the final score for that time point. Clasping behavior was scored on a 0–3 scale: a score of 0 indicated normal hind limb extension with no retraction; a score of 1 was assigned if one hind limb was retracted for at least 50% of the observation period; a score of 2 was given if both hind limbs were partially retracted for at least 50% of the time; and a score of 3 represented full retraction of both hind limbs for at least 50% of the trial.

At the study endpoint mice underwent a final clinical evaluation to quantify cumulative motor and neuropathological deficits. A clinical scoring system was used, adapted from previous studies (31), which ranged from 0 to 5. A score of 0 indicated a normal, healthy phenotype; 1 represented an unsteady gait; 2 reflected limb weakness or occasional tripping; 3 indicated severe limb weakness, though the

animal was still mobile and able to access food; 4 described a state of paralysis or profound weakness where movement was minimal or absent; and 5 indicated that the mouse was moribund or deceased.

Immunohistochemistry

Mice were euthanized and transcardially perfused with 0.1M phosphate-buffered saline (PBS) followed by 4% paraformaldehyde (PFA). Brains were post-fixed in 4% PFA for 24 hours and then cryoprotected in 30% sucrose. Coronal sections (30 µm thick) were prepared and stored in 0.1 M PBS containing 0.05% sodium azide until further use.

For brightfield immunohistochemistry, free-floating brain sections were first washed in 0.1 M phosphate-buffered saline (PBS) and quenched with 3% hydrogen peroxide to block endogenous peroxidase activity. Following additional washes, sections were incubated in a blocking solution containing 8% appropriate normal serum, 0.1% Triton X-100, and 0.1 M Tris-buffered saline (TBS-T) for 1 hour at room temperature. Sections were then incubated overnight at 4°C with primary antibodies against phosphorylated aSyn (p-aSyn) (Abcam, ab51253; 1:150,000) or tyrosine hydroxylase (TH) (Chemicon/Millipore, AB152; 1:2,500), diluted in 2% normal serum, 0.1 M TBS, and 50 µg/mL biotin (Vector Laboratories). To detect the insoluble form of p-aSyn, brain sections were incubated with proteinase K (PK; 10 µg/mL; MP Biomedicals, 183988) in 0.1 M TBS for 5 minutes at room temperature. The next day, sections were washed and incubated for 1 hour at 4°C with a biotinylated secondary antibody (Vector Laboratories) diluted in TBS-T. VectaStain® Elite ABC peroxidase kit (Vector Laboratories, PK-6100), and DAB kit (Vector Laboratories, SK-4100) were used according to the manufacturer's protocol to develop horseradish peroxidase activity. Stained sections were mounted onto Plus™ coated glass slides, dehydrated and coverslipped using permanent mounting medium (Vector Laboratories, H-5700-60).

Microscopy and Quantitative Image Analysis

Brightfield images for p-aSyn and TH were acquired using a Keyence BZ-X800 microscope. Images were taken at 20X magnification from cortex, striatum, SN, brainstem were captured for the analysis. NIHImageJ1.53 software (National Institute of Health) was used for quantification on the lesioned side. The total area of immuno-stained area with threshold parameters that excluded the background staining was detected. The average total area of the immuno-reactive area on each ROI for all images was plotted for analysis.

Stereological Analysis

Unbiased stereological estimation of TH-positive (TH^+) dopaminergic neurons in the SNpc was performed. SNpc was delineated using a 5× objective, and dopaminergic (DA) neurons were counted under a 40× objective using a Zeiss AxioImager M2 microscope. Serial coronal brain sections (30 µm thickness; mounted thickness ~22 µm) were placed six per slide. Every other slide was stained with TH and bisbenzimide for neuron identification. Stereological analysis was conducted using a systematic random sampling approach with counting frames (50 × 50 µm) overlaid on a sampling grid (190 ×

130 µm). Cells were counted within an 18 µm optical dissector, using 2 µm guard zones at the top and bottom of each section to avoid edge artifacts.

Western Blot Analysis of Spinal Cord Tissue

Spinal cord regions of interest were dissected from PFA-fixed tissue and transferred into 1.5 mL microcentrifuge tubes containing 150 µL of lysis buffer (300 mM Tris-HCl, pH 8.0, 2% SDS, 1% Triton X-100) supplemented with protease inhibitor cocktail (Roche). Tissues were sonicated at 30% amplitude using a cycle of 5 seconds on and 5 seconds off, repeated three times. Lysates were incubated at 100°C for 30 minutes followed by 80°C for 2 hours to enhance protein solubilization. After centrifugation, supernatants were collected for SDS-PAGE analysis. Protein samples were separated on 4–20% TGX Stain-Free gels (Bio-Rad) and imaged using the ChemiDoc MP system (Bio-Rad). Proteins were transferred to membranes and probed with anti-phospho-aSyn (p-aSyn; Abcam, ab51253), followed by HRP-conjugated secondary antibodies (1:2000; Jackson ImmunoResearch). Immunoreactive bands were detected using SuperSignal West Pico chemiluminescent substrate (Thermo Fisher Scientific) and quantified using Image Lab software (Bio-Rad).

Isolation of brain mononuclear immune cells for CyTOF Immunostaining

Mononuclear cells were isolated from mouse brains as previously described (26, 32). Briefly, mice were deeply anesthetized and perfused with PBS. Brains were extracted, minced in 3 mL of ice-cold 1× HBSS, and enzymatically digested in 3 mL of 2× dissociation medium containing DNase I (1 µL/mL; Invitrogen), Dispase II (1.2 U/mL; Roche), and Papain (1 mg/mL; Sigma-Aldrich) in DMEM/F12. Tissues were triturated using polished Pasteur pipettes of decreasing diameter, resuspended in 4 mL of 37 % isotonic Percoll (Sigma), and subjected to density gradient centrifugation using a 30:37:70 Percoll step gradient. Gradients were centrifuged at 500 × g for 30 minutes, and mononuclear cells were collected from the 37–70% interface. Cells were washed twice in HBSS, counted, and processed for CyTOF Immunostaining.

CyTOF Immunostaining

Single-cell suspensions were prepared from mouse spleen and brain tissue following PBS perfusion. After tissue dissociation and isolation, brain cells were pooled (n = 5–6) due to the low yield of immune cells from individual brains. In contrast, splenocytes were processed individually. Cells were washed and resuspended in Maxpar Cell Staining Buffer (CSB, Standard BioTools/Fluidigm, Cat# 201068). Cells were aliquoted and blocked Fc receptor by adding 5 µL of Mouse TruStain FcX (BioLegend, Cat# 422302). Meanwhile, surface marker cocktails containing 33 metal-conjugated antibodies (Maxpar OnDemand™ Mouse Immune Profiling Panel Kit, Cat# 92000001*)* and Cell-ID Intercalator-103Rh (2 µM final; Fluidigm) were prepared and incubated with cells for a 30-minute at room temperature. For fixation and DNA intercalation, cells were resuspended in 400 µL PBS and mixed with 400 µL of 2X Fix-IR solution containing isotonic paraformaldehyde, 2% saponin, Cell-ID Intercalator-Ir (125 µM; Fluidigm, Cat# S00093). Samples were incubated at room temperature for 30 minutes, followed by two washes with

CSB at 800 × g. Samples were resuspended in deionized water containing EQ™ Four Element Calibration Beads (Fluidigm) and acquired using a CyTOF XT mass cytometer. Brain immune profiles were analyzed using FlowJo software (version 10), and splenocyte populations were analyzed using Maxpar® Pathsetter™ software (version 3.0).

Primary cultures

Primary mixed neuron-glia cultures were prepared from the hippocampi of postnatal day 0–2 mice. Hippocampi were dissected, meninges removed under a stereomicroscope, and tissue minced and enzymatically digested in a solution containing 20 U/mL DNase I, 1 mg/mL papain, and 1.2 U/mL dispase II for 15 minutes at 37 °C. The reaction was quenched with fetal bovine serum (FBS), and cells were pelleted by centrifugation. Cells were resuspended in plating medium (Neurobasal A supplemented with 5% FBS, 2 mM Glutamax, and 10 µg/mL gentamycin), mechanically triturated using fire-polished glass pipettes, and filtered through a 40 µm cell strainer. Cells were seeded at 100,000 cells per 80 µL onto poly-D-lysine–coated coverslips (100 µg/mL) in 24-well plates. The next day, half of the medium was replaced with inhibitor medium containing 2 µg/mL aphidicolin to limit glial overgrowth. From that point, half-medium changes with culture medium (Neurobasal A + 1X B27 + 2 mM Glutamax) were performed every 4 days. On day 7, cultures were treated with sonicated aSyn PFF (PFFs; 1 µg/mL final concentration) or PBS. PFFs were prepared by mixing 10 µL of stock PFFs (4.38 mg/mL) with 10 µL PBS, followed by sonication. On day 14, primary NK cells were isolated from mouse spleen and added to selected wells at 10,000 cells/well (n= 6 per condition). Supernatants were collected after 24 hours for cytokine analysis using Meso Scale Discovery (MSD) assays, and cells were fixed on day 15 for immunostaining.

Primary microglial and astrocyte cultures were prepared from the cortices of postnatal day 3-6 (P3-P6) mouse pups (n=6-8). Cortical tissue was isolated, minced, and enzymatically dissociated in 0.25% Trypsin-EDTA at 37°C for 20 minutes with agitation every 5 minutes. Trypsin was neutralized with complete medium consisting of DMEM/F12 supplemented with 10% heat-inactivated fetal bovine serum (FBS; Sigma), 1% penicillin-streptomycin, and 1% L-glutamine (Sigma). The resulting cell suspension was plated and maintained at 37°C in 5% CO_2. For astrocyte cultures, cells were used after 4 days in vitro. For microglial isolation, mixed glial cultures were maintained for 12 days, after which microglia were harvested by mechanical agitation. Isolated microglia were replated in DMEM/F12 supplemented with 10% heat-inactivated FBS.

Bone marrow-derived macrophages (BMDMs) were generated as previously described (33). Briefly, bone marrow cells were isolated from the femurs and tibias of mice and cultured in DMEM/F12 supplemented with 10% fetal bovine serum (FBS) and 20% L929 cell-conditioned medium, which serves as a source of macrophage colony-stimulating factor (M-CSF), for 7 days. To reduce M-CSF signaling and minimize macrophage activation prior to experimentation, BMDMs were maintained in medium without L929-conditioned medium for an additional 2 days.

Immunocytochemistry

Primary neuron glia culture was incubated overnight at 4°C with anti-MAP2 (Invitrogen; 1:1000) and anti-p-aSyn (Abcam; 1:200) antibodies. Following primary incubation, cells were washed and incubated for 2 hours at room temperature (RT) with Alexa Fluor 594- and Alexa Fluor 488-conjugated secondary antibodies (Invitrogen; 1:1000). Coverslips were mounted using Fluoroshield Mounting Medium containing DAPI (Abcam). All fluorescent images were acquired using a Nikon A1R confocal microscope mounted on a Nikon Eclipse Ti-E inverted microscope platform.

Multiplex ELISA

Supernatants from primary cultures or serum samples were collected for cytokines and chemokines analysis. The Mouse Proinflammatory Panel 1 (Meso-Sacle Discovery, Gaithersburg, MD) was used to quantify IFNγ, IL-10, IL-12p70, IL-1, IL-2, IL-4, IL-5, IL-6, KC/GRO, and TNFα levels, following the manufacturer's instructions.

Quantitative Real-time RT-PCR (qPCR)

Total RNA was extracted from cultured cells using the RNeasy Mini Kit (Qiagen) and treated with DNase I to eliminate genomic DNA contamination. First-strand cDNA synthesis was performed using SuperScript II RNase H^- reverse transcriptase (Invitrogen). qPCR was conducted using SYBR Green Master Mix in a 384-well format on a QuantStudio 6 Real-Time PCR System (Thermo Fisher Scientific). Primer pairs were synthesized by Integrated DNA Technologies (IDT, Coralville, IA). The following primer sequences were used: *Mult1* (Forward: 5'-ACT GGC CAC ACA CCT CAG C-3', Reverse: 5'-TTC ACA TAG TGC AGG AGA CTA ACA CA-3'); *Qa-1a* (Forward: 5'-TCT GTG AGG CAA AGT CAG TC-3', Reverse: 5'-GCG GTA TTT CCA CAC TGC CA-3'); *Qa-1b* (Forward: 5'-CAC CAC AGC TCC AAG GAT GAT-3', Reverse: 5'-CCT GGA CCG CGA ATG ACA TA-3'); *Rae-1* (Forward: 5'-AGA TAT GAA GAT GAG TCC CAC AGA GAT A-3', Reverse: 5'-ATC AAC TTC CCC GCT TCC A-3'); *H60* (Forward: 5'-CCA GTA TGG TCC CCA GAT AGC T-3', Reverse: 5'-GAG CCA CCA GCA AGA GCA A-3'); *p16* (Forward: 5'-TGT TGA GGC TAG AGA GGA TCT TG-3', Reverse: 5'-CGA ATC TGC ACC GTA GTT GAG C-3'); and *p21* (Forward: 5'-TCG CTG TCT TGC ACT CTG GTG T-3', Reverse: 5'-CCA ATC TGC GCT TGG AGT GAT AG-3'). All reactions were run in triplicate, and relative expression was calculated using the ΔΔCt method, normalized to housekeeping genes. Each reaction was run in triplicate, and data are presented as mean ± SEM.

Statistical Analysis:

Statistical analyses were conducted using GraphPad Prism 10 software. Data are presented as mean ± SEM. Comparisons between treatment groups were performed using two-way ANOVA followed by Tukey's multiple comparisons test or Fisher's LSD post-hoc test. Comparisons within groups were analyzed using one-way ANOVA or Student's unpaired t-test. A p-value of < 0.05 was considered statistically significant.

RESULTS

Systemic NK cell transfer increases NK1.1⁺ cells in recipient mice.

To evaluate the effects of NK cell transfer therapy in a mouse model of neurodegenerative disease, we stereotaxically injected 2-month-old homozygous M83 Tg mice (both males and females) with 5 µg of human αSyn PFF or monomeric αSyn into the striatum. To preserve NK cell phenotype and function, untouched NK cells were isolated from the spleens of background-matched B6C3F1/J mice (2–4 months old) using a negative selection approach (EasySep™ Mouse NK Cell Isolation Kit). NK subset analysis based on CD11b and CD27 markers revealed that the majority of enriched NK cells exhibited $CD11b^{+}CD27^{-}$ and $CD11b^{+}CD27^{+}$ phenotypes **(Supplementary Fig. S1)**.

Given the turnover rate of circulating human NK cells and adoptively transferred murine NK cells (~ 7–14 days) (34–36), NK cells were administered intraperitoneally (i.p.) at two-week intervals to maintain consistent immunological pressure throughout disease progression. The dosing regimen (2 or 4 million cells per injection) and infusion timeline were adapted from previously validated protocols (35, 37). Successful engraftment of $NK1.1^{+}$ cells in recipient mice confirmed the efficacy of this systemic delivery strategy. $NK1.1^{+}$ populations were substantially elevated in both the spleen and circulating blood of NK-treated mice compared to saline-treated controls **(**Fig. 1e**)**, demonstrating that intraperitoneally administered NK cells can persist and expand in vivo. This engraftment established a robust immunological foundation for further evaluating NK cell–mediated modulation of αSyn pathology, neuroinflammation, and neuronal survival. Motor function was assessed biweekly following NK cell administration. Tissues were harvested at Weeks 7 and 11 post-injections for analysis of αSyn pathology, neuroinflammation, and therapeutic responses **(**Fig. 1a**)**. The conformations of αSyn species (monomer, PFF, and sonicated PFF) were validated by transmission electron microscopy **(**Fig. 1b**)**, and TLR4 reporter assays using HEK293 cells confirmed minimal biological activity of the αSyn preparations **(**Fig. 1c**)**.

NK cell transfer ameliorates motor deficits, α-syn burden and neurodegeneration in the α-Syn PFF M83 mouse model.

To determine whether NK cell infusion modulates disease progression in α-synucleinopathy, we assessed motor function and neuropathology in M83 Tg mice injected with aSyn PFF (PFF) or monomeric aSyn (Mono). Hind limb clasping scores were recorded biweekly. Mice treated with PFF and saline (PFF/Saline) exhibited the most severe motor impairments, with scores approaching 2.0 by Week 10. In contrast, PFF-injected mice treated with NK cells (PFF/NK) showed a dose-dependent protective effect, with the 4 million NK cell group demonstrating the greatest improvement **(**Fig. 2a**)**. Clinical scores were assessed at the endpoint (11 weeks) as the homozygous M83 Tg mice injected with aSyn PFF typically display symptom onset around 10 weeks post-injection, followed by a rapid clinical decline within a few days, as previously observed (28). Due to this late onset and fast progression, scores were recorded on the day of sacrifice. Clinical scores, revealed that over 50% of PFF/Saline mice developed severe symptoms (scores 3–5). Interestingly, PFF/NK mice exhibited similar levels of clinical severity at this late stage, indicating limited therapeutic benefit of NK cells during advanced disease **(**Fig. 2b**).**

We next evaluated aSyn pathology by performing immunohistochemistry for proteinase K (PK)-resistant p-aSyn. Our data revealed extensive aSyn inclusions in the cortex, striatum, substantia nigra (SN), and brainstem of PFF/Saline mice at 11 weeks (Fig. 2c). NK cell infusion (4 million) significantly reduced aSyn pathology in the SN (*p < 0.05) and brainstem (**p < 0.01) compared to PFF/Saline. A modest increase in striatal pathology was observed. Notably, in the monomer-injected NK-treated group (Mono/NK), high-dose NK cell infusion reduced aSyn pathology in the striatum (*p < 0.05), SN (*p < 0.05), and brainstem (**p < 0.01) compared to monomer-injected saline-treated controls (Mono/Saline). The cortex showed a reduction trend, but it did not reach statistical significance (Fig. 2c). We also observed that low-dose NK cell infusion (2 million) also led to significant reductions aSyn pathology, particularly in striatal (**p < 0.01) and SN (*p < 0.05). aSyn pathology across both PFF and monomer-injected groups. No significant differences were observed in the cortex or brainstem **(Supplementary Fig. 2)**.

Stereological quantification of tyrosine hydroxylase (TH)-positive neurons in the SNpc revealed that PFF/Saline treatment caused an approximately 47% reduction in dopaminergic neurons compared to Mono/Saline ($p < 0.05$) (Fig. 2d, e). PFF/NK mice exhibited significantly higher TH^+ neuron counts compared to the PFF/Saline group, indicating NK cell-mediated neuroprotection. In contrast, NK cell infusion in the absence of PFF (Mono/NK) had no significant effect, suggesting the protective action is context-dependent.

To assess aSyn pathology along the spinal cord, we performed quantitative immunoblotting of p-aSyn at Week 7 post-injection across lumber, thoracic, and cervical regions. In the lumbar spinal cord, PFF/NK mice exhibited a ~ 60% reduction in aSyn pathology compared to PFF/Saline, restoring levels to those of Mono/Saline controls (Fig. 2f, g). A similar, though less pronounced, reduction was observed in the thoracic region (Fig. 2h, **Supplementary Fig. 3a)**. In the cervical region, a reduction in aSyn levels was also noted in PFF/NK mice; however, this difference did not reach statistical significance (Fig. 2i, **Supplementary Fig. 3b)**. These results suggest a rostrocaudal gradient in NK cell efficacy, with maximal benefit in the lumbar spinal cord and limited effect in the cervical region at this time point.

NK cell transfer reduces neuroinflammation and peripheral cell infiltration in the CNS in the α-Syn PFF M83 mice.

To investigate NK cell-mediated immune changes in the CNS and periphery, we performed mass cytometry (CyTOF) using metal-tagged antibodies to profile immune cell populations in the brain at 7 weeks post-injection - a time point selected based on peak behavioral improvement following NK cell treatment. To ensure analysis of CNS-resident and infiltrating immune cells, mice were perfused with PBS prior to tissue collection to remove circulating blood cells (Fig. 3a).

In the Mono/Saline control group, B cells accounted for 1.17% of the total brain immune cells, while T cells comprised 9.31%. NK cell infusion in monomer-injected mice (Mono/NK) increased B cell frequency nearly six-fold (6.85%) and elevated T cells to 15.4%. In the PFF/Saline group, B cell levels remained low (1.43%), but T cells rose to 14.2%. Notably, NK cell treatment in PFF-injected mice (PFF/NK) led to a striking expansion of $CD19^+$ B cells to 12.6%-a nearly ninefold increase compared to

PFF/Saline controls (Fig. 3c). This pronounced B cell expansion suggests that NK cells may promote B cell–mediated immune responses during synucleinopathy.

T cell subset analysis revealed additional NK cell–driven changes. In Mono/Saline mice, $CD4^+$ T cells were dominant (29.3%) over $CD8^+$ T cells (5.48%). NK cell transfer (Mono/NK) decreased $CD4^+$ T cells to 16.3% and increased $CD8^+$ T cells to 6.46%. In the PFF/Saline group, $CD4^+$ T cells remained elevated (28.8%), while $CD8^+$ T cells declined to 3.14%, suggesting limited recruitment of cytotoxic T cells. Importantly, the PFF/NK group reversed this pattern, reducing $CD4^+$ T cells to 10.4% (a 64% reduction vs. PFF/Saline), and increasing $CD8^+$ T cells to 9.15% (Fig. 3d). In addition, saline-injected controls mice (Fig. 3b) exhibited low baseline frequencies of CD4 + T cells (10.8%) and $CD8^+$ T cells (2.01%), suggesting that monomeric aSyn may alter CNS immune composition.

We next analyzed CD11b and CD45 expression within the non-B non-T and CD11 + myeloid population. We found that NK cell infusion significantly reshaped the myeloid landscape. In Mono/Saline mice, neutrophils ($CD11b^+Ly6G^+$) dominated in Mono/Saline mice (65.6%), while $CD11b^+Ly6G^-$ myeloid cells (including monocytes, macrophages, and microglia) constituted 25.5%. NK cell infusion (Mono/NK) dramatically reduced neutrophils to 24.5% and expanded $CD11b^+Ly6G^-$ cells to 51.9%. Saline-injected non-surgery baseline controls mice shown in the gating strategy (Fig. 3b) showed 25.5% neutrophils and 64.4% myeloid cells, reinforcing the notion that monomeric aSyn can modulate immune homeostasis. In PFF/Saline mice, neutrophils (42.5%) and myeloid cells (41.7%) were nearly equal, whereas NK cell infusion (PFF/NK) resulted in the most pronounced effect: reducing neutrophils to 16.3%, and increasing $CD11b^+Ly6G^-$ cells to 64.5% similar to the levels observed in controls (Fig. 3e).

We also analyzed CD11b and CD45 expression within the non-B non-T and Ly6G- myeloid population, representing primarily microglia and infiltrated macrophages. In Mono/Saline mice, 63.3% of cells were $CD11b^+CD45^{low}$ (homeostatic microglia), and 31.8% were $CD11b^+CD45^{high}$ (activated microglia/infiltrated macrophages). PFF injection (PFF/Saline) shifted this ratio, decreasing $CD45^{low}$ cells to 51.3% and increasing $CD45^{high}$ cells to 43.1% (Fig. 3f). NK cell infusion (PFF/NK) reversed this pattern, restoring $CD45^{low}$ cells to 84.8% and reducing $CD45^{high}$ cells to 13.3%—a 69% reduction compared to PFF/Saline. MHCII expression, a marker of myeloid activation, similarly varied across groups. PFF/Saline mice showed the highest $MHCII^+$ myeloid cell frequency (32.4%), nearly double that of Mono/Saline (17.0%). NK cell treatment suppressed MHCII expression in both monomer- and PFF-injected mice, with PFF/NK mice showing a 62% reduction in $MHCII^+$ cells (12.2%) compared to PFF/Saline (Fig. 3g). In contrast, CD11c expression, associated with disease-associated microglia/macrophages (DAMs), was lowest in Mono/Saline (6.29%) but increased with PFF injection (13.5%). Interestingly, NK treatment further elevated $CD11c^+$ cells in PFF/NK mice to 18.2%, a 35% increase compared to PFF/Saline, suggesting that NK therapy may promote a beneficial DAM-like phenotype during aSyn pathology. For baseline comparison, saline-injected non-surgery control mice shown in the gating strategy exhibited 84.7% $CD11b^+CD45^{low}$, 10.1% $CD11b^+CD45^{hig}$ cells, 6.88% of $MHCII^+$ myeloid and 2.87% $CD11c^+$ cells (Fig. 3b), further supporting the idea that monomeric aSyn

subtly disrupt CNS immune homeostasis. Importantly, NK cell infusion in both PFF- and monomer-injected mice restored homeostatic immune profile to baseline level.

Finally, we assessed NK cell presence and phenotype post-transfer. $CD335^+$ ($NKp46^+$) NK cells were low in Mono/Saline (1.35%) and PFF/Saline (1.56%) but significantly increased following NK treatment in both Mono/NK (7.48%) and PFF/NK (3.28%) mice (Fig. 3i). Despite successful engraftment, levels were lower in the PFF context, suggesting reduced persistence or recruitment. NK-treated groups showed high proportions of immature $CD11b^-CD27^-$ NK cells (~ 70%) and a reduction in mature $CD11b^+CD27^-$ subsets. Terminally differentiated $CD11b^+CD27^+$ NK cells were nearly absent across all groups (Fig. 3j).

A heatmap summarizing immune subset abundance (Fig. 3k) highlights the PFF/NK group's distinct immune profile: elevated $CD19^+$ B and $CD8^+$ T cells, reduced $CD4^+$ T cells and neutrophils, decreased activated microglia, and increased NK cells. Together, these changes suggest a coordinated, potentially neuroprotective immune response facilitated by NK cell therapy in synucleinopathy.

NK cells directly modulate neuroinflammatory responses in aSyn-challenged primary neuron-glia cultures

Given the systemic immunomodulatory effects observed with NK cell infusion in vivo, we next investigated whether NK cells could directly modulate immune responses in neuron-glia culture under aSyn-induced stress. Mixed neuron-glia cultures were established from postnatal day 0–2 mouse hippocampi. On day 7 in vitro, cultures were treated with either PBS or sonicated aSyn (aSyn PFFs; 1 µg/mL). On day 14, primary NK cells, isolated from mouse spleens, were added to the cultures. Supernatants were collected 24 hours later for multiplex cytokine analysis (Fig. 4a). Co-culture of NK cells with aSyn-treated neuron-glia cultures induced measurable changes in the inflammatory milieu, with distinct cytokine signatures emerging across treatment conditions (Fig. 4b). TNFα levels were comparable between PBS and aSyn-treated cultures, indicating that aSyn did not further elevate TNFα beyond baseline. However, NK cell addition significantly reduced TNFα in both PBS and aSyn-treated cultures (~ 8–10 pg/mL), demonstrating NK-mediated suppression of both basal and aSyn-induced TNFα production (Fig. 4b). IL-10 levels remained elevated (~ 8–13 pg/mL) following both PBS and PFF treatments, suggesting preserved anti-inflammatory tone. NK cell co-treatment led to a reduction in IL-10 levels across both conditions, indicating NK cell–mediated downregulation of IL-10 expression (Fig. 4b). IL-12p70 exhibited context-dependent modulation. While low in PBS-only cultures, NK treatment modestly increased IL-12p70 under baseline conditions. aSyn exposure significantly upregulated IL-12p70, and NK cells reduced this elevation back to baseline, indicating suppression of pathology-driven IL-12p70 induction (Fig. 4b).

IL-4 levels were low in PBS cultures (~ 0.05 pg/mL) but increased with NK co-treatment (~ 0.2 pg/mL), suggesting NK cell–driven IL-4 production in healthy conditions. In contrast, this NK cell–driven IL-4 induction was lost in aSyn-treated cultures (Fig. 4b). IL-6 levels were significantly elevated in PBS/NK and aSyn/NK groups (~ 100–150 pg/mL) compared to PBS-only (~ 60–90 pg/mL), indicating that NK

cell infusion enhances IL-6 production regardless of aSyn challenge (Fig. 4b). In contrast, PFF alone did not significantly increase IL-6 compared to PBS, suggesting that the observed elevation is specifically driven by NK cell presence rather than aSyn pathology alone. This implies that NK cells may promote IL-6 production as part of a broader immunomodulatory response in both healthy and pathological conditions (Fig. 4b).

KC/GRO (CXCL1) levels showed substantial variability across treatment groups, with mean values trending higher in the aSyn group and lower in the PBS + NK group. One-way ANOVA revealed a trend toward significance ($p = 0.069$), though not statistically significant (Fig. 4b). Despite this, group means suggest that aSyn exposure elevates KC/GRO, a chemokine associated with neutrophil recruitment, while NK cell treatment in both PBS + NK and PFF + NK groups modestly reduced KC/GRO levels relative to their respective controls (Fig. 4b). These reductions did not reach statistical significance in post hoc tests, but the trend is consistent with other findings showing that NK cells attenuate inflammatory chemokine signals. No significant differences were observed in IL-1β levels across treatment conditions, while IL-2 showed preferential elevation in the PBS + NK group compared to other conditions (Fig. 4b), suggesting NK cells primarily stimulate this pathway in non-pathological settings.

These results collectively show that NK cells modulate specific inflammatory pathways in a context-dependent manner, suppressing pro-inflammatory mediators (e.g., TNFα, IL-12p70) and enhancing select immune regulators (e.g., IL-4, IL-2) predominantly in healthy environments. The ability of NK cells to dampen aSyn–induced cytokine responses suggest a direct immunomodulatory role in neural cultures.

Immunofluorescence imaging revealed intact neuronal networks in PBS controls, with extensive neurite outgrowth and normal morphology. αSyn treatment induced notable neuronal damage, characterized by neurite fragmentation and abnormal cellular aggregates. NK cell addition to aSyn-challenged cultures partially preserved neuronal integrity and network complexity, suggesting neuroprotective effects (Fig. 4c).

aSyn alters NK cell ligand expression and induces senescence-associated profiles in neural and myeloid cells.

NK cells, unlike T and B cell, do not undergo somatic gene rearrangement. Instead, they express a diverse repertoire of activating and inhibitory receptors (NKRs) that collectively determine whether they are activated or restrained (38). Stress-inducible ligands such as retinoic acid early transcripts α-ε (RAE-1 α-ε), murine UL16-binding protein-like transcript 1 (MULT1), H60 a-c in mice are recognized by the NKG2D receptor on NK cells, triggering cytotoxic responses against damaged or abnormal cells (39). In contrast, the inhibitory ligand mQa1b engages the NKG2A/CD94 receptor complex on NK cells, delivering suppressive signals that prevent inappropriate NK activation (40). Changes in the expression of these ligands can modulate NK cell recognition and the clearance of affected neural and myeloid cells.

To investigate whether aSyn pathology impact NK cell surveillance, we assessed the expression of NK cell receptor ligands across major CNS and myeloid cell types. Primary cultures of microglia, neurons,

astrocytes, and bone marrow-derived macrophages (BMDMs) were exposed to aSyn exposure, and the expression levels of activating and inhibitory ligands were evaluated. In parallel, we examined the induction of senescence-associated markers, as cellular senescence may promote immune evasion and sustain chronic inflammation during neurodegenerative disease progression (Fig. 5). In primary microglia, treatment with aSyn (40 μg/mL) significantly downregulated the activating NK cell ligands mRae1 and mH60 by approximately 85% and 45%, respectively, compared to untreated controls ($p < 0.0001$). Conversely, the inhibitory ligand mQa1b was upregulated nearly 5-fold ($p < 0.0001$), while mMult1 expression remained unchanged (Fig. 5a). This ligand shift suggests that aSyn exposure drives microglia toward an NK cell–resistant phenotype. Additionally, the senescence marker p21 was robustly induced (> 4-fold, $p < 0.0001$), while p16 levels remained unaffected, indicating selective activation of senescence-related pathways (Fig. 5e). Neurons, exposed to a lower dose of aSyn (1.5 μg/mL), showed significant downregulation of all activating NK cell ligands (mRae1, mH60, and mMult1; $p < 0.01 – 0.001$), suggesting reduced visibility to NK cells (Fig. 5b). However, neither the inhibitory ligand mQa1b nor senescence markers (p16, p21) were significantly altered, indicating a cell type–specific and ligand-specific response to aSyn (Fig. 5f). Astrocytes demonstrated remarkable resistance to aSyn–induced changes. Even under high-dose aSyn exposure (40 μg/mL), expression of all NK cell receptor ligands remained unchanged (Fig. 5c), suggesting that astrocyte–NK cell interactions may remain stable during pathological conditions. BMDMs exhibited the most pronounced and dose-dependent responses to aSyn exposure. Activating ligands mRae1, mH60, and mMult1 were progressively downregulated ($p < 0.05–0.0001$), while the inhibitory ligand mQa1b was upregulated over 3-fold at the highest dose ($p < 0.0001$) (Fig. 5d). In contrast to microglia, the senescence markers p16 and p21 exhibited opposite trends: p16 levels increased modestly with aSyn dose, while p21 decreased slightly. However, neither change reached statistical significance, suggesting that aSyn exposure alters NK ligand expression but not senescence-associated markers in BMDMs (Fig. 5g).

Collectively, these data reveal that aSyn alters the immunological landscape of neural and myeloid cells by shifting NK receptor ligand expression toward an inhibitory state, while selectively inducing senescence markers. These changes suggest that aSyn may promote senescence-like phenotypes that limit immune clearance. This mechanism may contribute to chronic neuroinflammation and persistent pathology in synucleinopathies.

Systemic NK cell transfer modulates peripheral immunity by increasing follicular B cells and reducing neutrophils without inducing systemic immunotoxicity.

To assess the systemic immune effects of NK cell therapy, we performed high-dimensional CyTOF mass cytometry on splenic $CD45^+$ cells from the same mice analyzed in Fig. 3. The profiling revealed distinct immune cell clusters and treatment-dependent alterations in immune composition (Fig. 6a). $CD4^+$ T cell subset analysis revealed no significant changes across treatment groups. Frequencies of naïve ($CD4^+$ NV), central memory ($CD4^+$ CM), effector memory ($CD4^+$ EM), PD-1^+ $CD4^+$ T cells, and regulatory T cells ($CD4^+$ Tregs) remained consistent regardless of NK cell infusion or aSyn PFF exposure, indicating that neither intervention significantly modulates splenic $CD4^+$ T cell composition (Fig. 6c). Splenic profiling of

$CD8^+$ T cell subsets revealed minimal changes across treatment groups. Naïve $CD8^+$ T cells (CD8 NV) showed modest variability within groups, with no consistent pattern of expansion or reduction associated with either NK cell infusion or PFF exposure. Central memory (CD8 CM) and effector memory (CD8 EM) subsets were present at low frequencies across all conditions, though a slight increase in CD8 EM cells was noted in NK-treated animals (up to 1.6% in Mono NK and 1.3% in PFF NK), suggesting a possible trend toward enhanced memory activation with NK therapy (Fig. 6d). B cell subset analysis revealed a clear NK cell–mediated modulation, especially within the follicular (FO) B cell compartment. FO B cell frequencies, reduced in PFF/Saline mice (22.4–29.9%) compared to Mono/Saline (up to 33.6%), were restored and expanded in both Mono/NK and PFF/NK groups (up to 40.5% and 36.7%, respectively), suggesting NK cell-driven support for B cell homeostasis. Plasmablasts also increased in NK-treated groups (up to 1.2%), whereas B1, B1a, and B1b cells remained consistently low across all conditions therapy (Fig. 6e). Analysis of splenic NK subsets showed that adoptively transferred NK cells skew toward immature phenotypes by day 7 post-infusion. Mature cytotoxic subsets ($CD11b^+CD27^+$ and $CD11b^+CD27^-$) were substantially reduced or nearly absent in NK-treated animals, while immature subsets ($CD11b^-CD27^-$ and $CD11b^-CD27^+$) were more prominent, particularly in Mono NK. PFF/NK animals showed an overall reduction in NK subsets, suggesting aSyn pathology may limit NK cell expansion or persistence. These findings align with established literature indicating limited in vivo persistence (~ 7–14 days) of adoptively transferred NK cells (Fig. 6f). Neutrophil frequencies were significantly reduced in NK-treated animals compared to saline-treated controls: Mono/NK (0.8–3.8%) vs. Mono/Saline (2.7–10.2%), and PFF/NK (0.9–6.3%) vs. PFF/Saline (1.6–11.2%) (Fig. 6h). This suggests NK cells may suppress neutrophil expansion or infiltration, potentially mitigating pro-inflammatory responses. However, the effect appeared less robust in the PFF/NK group, possibly due to ongoing neuroinflammatory stimuli. Unconventional T cells showed modest treatment-associated changes. NKT cells remained consistently low (~ 0.1–0.2%) across all groups. γδ T cells showed more variability, with a mild expansion in some PFF/NK mice (up to 1.7%), suggesting that NK cells may influence this population in certain inflammatory contexts (Fig. 6g).

Importantly, spleen size did not differ between groups, indicating that NK cell infusion does not induce splenomegaly or systemic immunotoxicity (Fig. 6j). Finally, serum cytokine profiling at 11 weeks post-injection revealed no major differences in inflammatory cytokines across groups. While some individual outliers were present, median cytokine levels remained comparable between NK- and saline-treated animals, supporting the immune tolerability of adoptive NK cell therapy (Fig. 7).

Discussion

We previously established a progressive synucleinopathy model by inoculating aSyn PFF into M83 Tg mice (27). These mice develop extensive aSyn pathology and exhibit pronounced motor deficits and nigrostriatal neurodegeneration, making them well-suited for modeling both functional and pathological aspects of disease. Importantly, disease phenotypes emerge within 2–3 months post-injection, enabling timely evaluation of therapeutic interventions such as NK cell therapy. Our results demonstrate that systemic NK cell transfer mitigates key pathological and functional hallmarks of synucleinopathy in the

PFF-injected M83 model. NK cell therapy provided dose-dependent motor benefit, as evidenced by reduced hindlimb clasping scores, with the higher dose (4 million cells) conferring the greatest functional improvement. This protective effect was observed during the early to mid-phase of disease progression. However, clinical scoring at the terminal stage (11 weeks) revealed limited efficacy in halting end-stage decline, suggesting that NK cell therapy may be more effective prior to the onset of irreversible neurodegeneration. Pathological assessment confirmed that NK cells modulate aSyn burden in a region- and context-specific manner. In PFF-injected mice, high-dose NK treatment significantly reduced p-aSyn pathology in the SN and brainstem, regions critical for motor control. Conversely, a modest increase in striatal pathology was noted at later time points in PFF/NK mice, possibly reflecting regional differences in NK cell infiltration, immune activation thresholds, or local microenvironmental factors. Interestingly, in the monomer-injected group (a milder model), NK cells reduced pathology across multiple brain regions, suggesting that NK-mediated clearance may be more effective under conditions of lower aggregate burden or earlier disease stages.

In the spinal cord, NK cell infusion reduced aSyn pathology most robustly in the lumbar region, with a decreasing gradient toward the cervical region. This rostrocaudal gradient may reflect differential trafficking or functional persistence of transferred NK cells, regional differences in aSyn propagation, or variable accessibility across the CNS axis. Such spatially distinct efficacy could inform region-targeted delivery strategies or adjunctive therapies to enhance global CNS protection.

$CD4^+$ T cells are key drivers of neuroinflammation and neurodegeneration in aSyn-based models, promoting myeloid activation and dopaminergic neuron loss, effects mitigated by their depletion (11, 41). While $CD8^+$ T cells also infiltrate the CNS and are abundant at the blood-brain barrier, knockout studies suggest they are not essential for neurodegeneration in some models (11). Recent studies highlight a protective role for B cells in PD model. Specifically, B cell depletion in the 6-hydroxydopamine (6-OHDA) lesion model leads to worsened motor deficits and exacerbated dopaminergic neuron loss (42). Using high-dimensional CyTOF analysis, we demonstrated that NK cell infusion profoundly influenced both lymphoid and myeloid compartments, revealing a broad immunomodulatory capacity that extends beyond NK cell effector functions alone. Both $CD4^+$ and $CD8^+$ T cells contribute to PD, though their roles differ across models. One of the most intriguing immunological effects of NK cell therapy was the expansion of $CD19^+$ B cells, particularly in the PFF/NK group, suggesting that NK cells may promote B cell recruitment or survival within the inflamed CNS. This was accompanied by a notable shift in T cell composition: an increase in $CD8^+$ T cells and a concurrent reduction in $CD4^+$ T cells, indicative of a more cytotoxic and potentially immunoregulatory environment. A similar pattern of immune modulation was observed in the periphery. In the spleen, NK cell therapy restored and expanded follicular B cell populations that were otherwise reduced in PFF/Saline mice. This suggests that NK cells contribute to humoral immune homeostasis, potentially through cytokine signaling or secondary lymphoid organ remodeling.

Neutrophils have been increasingly recognized as key contributors to PD pathogenesis, promoting systemic inflammation, oxidative stress, and blood-brain barrier (BBB) disruption (43). Elevated

neutrophil-to-lymphocyte ratios (NLR), a marker of systemic inflammation, are consistently correlated with PD severity and dopaminergic neurodegeneration (44). Our findings provide compelling evidence that NK cell therapy directly counteracts this neutrophil-driven inflammatory axis. Specifically, we observed a robust reduction in neutrophil frequencies both centrally and peripherally following NK cell infusion, under both monomer and PFF aSyn conditions. This suggests that NK cells exert broad immunoregulatory effects capable of dampening pro-inflammatory myeloid responses. Importantly, NK cell treatment significantly decreased the abundance of $CD11b^{+}CD45^{high}$ cells - activated microglia/macrophages - and restored the homeostatic $CD45^{low}$ microglial pool, suggesting resolution of microglial activation. This is further supported by a marked decrease in MHCII expression, indicating suppressed antigen-presenting activity and possibly attenuated neuroinflammation. Interestingly, $CD11c^{+}$ myeloid populations increased following NK infusion in PFF mice, suggesting the emergence of a "disease-associated microglia" (DAM)-like phenotype (45), which has been proposed to play protective roles in neurodegeneration by enhancing phagocytosis and limiting inflammation. The enrichment of this population may reflect a beneficial reprogramming of CNS-resident immune cells. Importantly, NK cell infusion in both PFF- and Mono-injected mice effectively reestablished baseline homeostatic immune profiles, highlighting its potential to normalize CNS immune dysregulation.

Direct evidence of NK cell engraftment in the brain was confirmed by increased frequencies of $CD335^{+}$ ($NKp46^{+}$) cells following NK cell transfer. Notably, the predominance of immature ($CD11b^{-}CD27^{-}$) NK cell phenotypes in both the Mono/NK and PFF/NK groups suggests that NK cells may either undergo phenotypic shifts within the CNS or preferentially infiltrate in a less mature state. Immature NK cells are thought to possess heightened cytokine production with limited cytotoxic activity, features that could be particularly beneficial in the inflamed or degenerating CNS by promoting immunomodulation rather than cytotoxic damage. Thus, the enrichment of $CD11b^{-}CD27^{-}$ NK cells in the brain may represent a specialized, neuroprotective subset that adapts to the CNS microenvironment. Alternatively, the reduced NK cell levels observed in PFF/NK mice could reflect impaired CNS homing or diminished persistence under inflammatory conditions, potentially limiting therapeutic durability at later disease stages. Our In vitro data further demonstrated that NK cells exert immunomodulatory effects in the context of aSyn–induced neuroinflammation. Co-culture of NK cells with aSyn PFF-challenged neuron-glia cultures significantly altered cytokine profiles, suggesting that NK cells actively reshape the inflammatory environment. This may reflect efforts to resolve inflammation without promoting compensatory immune suppression.

NK cells play a regulatory role in CNS inflammation by targeting autoimmunogenic T cells and activated microglia with reduced expression of Qa-1, the murine homolog of HLA-E, which normally binds the inhibitory NKG2A receptor on NK cells to suppress cytotoxicity (46, 47). NK cells also mediate cytotoxicity against immature or damaged neurons, including dorsal root ganglion neurons that express RAE1, a ligand for the activating NKG2D receptor (48, 49). We demonstrated that aSyn exposure induced a marked shift in NK ligand expression across multiple cell types: activating ligands such as Rae1, H60, and Mult1 were significantly downregulated, while the inhibitory ligand mQa1b was upregulated—

particularly in microglia and BMDMs. This pattern suggests that aSyn pathology promotes an immunoevasive phenotype that may impair NK cell–mediated clearance of damaged or senescent cells. These findings align with the broader concept of immune privilege in chronic neurodegeneration, where persistent inflammation paradoxically dampens immune surveillance and contributes to disease progression.

In primary microglia exposed to aSyn, p21-but not p16-was upregulated, consistent with prior reports showing aSyn PFF-induced p21 elevation in reactive glia in mouse models (50). This selective induction suggests a partial senescence-like state, which may sustain chronic inflammation and impair immune clearance without triggering full cellular senescence. Such a phenotype aligns with the concept of a senescence-associated secretory profile (SASP) and may have important implications for persistent neuroinflammation in synucleinopathies. Given these findings, it is plausible to hypothesize that the progressive accumulation of senescence-like cells, coupled with persistent inflammation, could contribute to the diminished effectiveness of NK cell infusion therapies at later disease stages. Despite substantial immunological reprogramming in the CNS and periphery, serum levels of inflammatory cytokines remained largely unchanged across treatment groups. The lack of systemic cytokine storm or inflammatory signatures supports the tolerability of repeated NK cell dosing.

Conclusion

Collectively, our findings highlight NK cells as multifaceted immunomodulators capable of targeting disease-relevant mechanisms across both central and peripheral compartments. By attenuating aSyn pathology, suppressing maladaptive inflammation, and restoring immune balance without inducing systemic toxicity, NK cell therapy emerges as a promising, well-tolerated, and mechanistically targeted intervention for synucleinopathies. Further studies are warranted to enhance NK cell persistence, optimize dosing strategies, and explore combinatorial approaches to achieve durable disease modification.

Abbreviations

BBB: Blood-brain barrier

BMDMs: Bone marrow-derived macrophages

CD: Cluster of differentiation

CM: Central memory

CNS: Central nervous system

CSF: Cerebrospinal fluid

CyTOF: Cytometry by time of flight (Mass cytometry)

DAMs: Disease-associated microglia

EM: Effector memory

FO: Follicular

HLA-E: Human leukocyte antigen-E

H60: Histocompatibility 60

IL: Interleukin

KC/GRO: Keratinocyte chemoattractant/Growth-regulated oncogene

MHC II: Major Histocompatibility Complex II

mQa1b: Murine homolog of HLA-E

MULT1: Murine UL 16-binding protein-like transcript 1

NK: Natural killer

NKG2A or NKG2D: Natural killer group 2 member A or D protein

NLR: Neutrophil-to-lymphocyte Ratios

NKT: Natural Killer T cells

NV: Naïve

PD: Parkinson's disease

PFF α-syn: Preformed fibril α-synuclein

PK: Proteinase K

p-aSyn: Phosphorylated α-synuclein at serine 129

RAE-1: Retinoic acid early inducible 1

SASP: Senescence-associated secretory profile

SN: Substantia nigra

SNpc: Substantia nigra pars compacta

STR: Striatum

TCR: T-cell receptor

TEM: Transmission electron microscopy

Tg: Transgenic

TH: Tyrosine Hydroxylase

TLR: Toll-like receptor

TNF: Tumor necrosis factor

Tregs: Regulatory T cells

Declarations

Ethics approval and consent to participate: All animal procedures were performed in accordance with NIH guidelines and with the approval of the University of Georgia Institutional Animal Care and Use Committee prior to all animal-related studies (IACUC protocol AUP #: A2024 11-008-Y1-A0).

Consent for publication: All authors have approved the contents of this manuscript and provided consent for publication.

Availability of data and materials: The data supporting the findings of this study are available from the corresponding authors upon request.

Competing Interests: A.A., B.J., C.J., and G.D. declare no competing interests. L.J.K. serves as a scientific advisor for Neuronity Therapeutics, Inc. L.H.J. is a founder of Neuronity Therapeutics, Inc.

Funding: This study was supported by awards to JKL by the NIH R01NS119610.

Author Contributions: L.J.K. designed the study and supervised the research. A.A. performed the animal experiments, including NK cell infusion, behavioral testing, and flow cytometry. B.J. conducted all immunohistochemical experiments and analyses. C.J. performed the in vitro cultures, assays, and MSD ELISA experiments. L.J.K. and L.H.J. carried out the stereotaxic surgeries. L.J.K. also performed the CyTOF experiments and subsequent data analysis. G.D. and L.J. participated in and assisted with experimental procedures. L.J.K., A.A., B.J., and C.J. wrote the manuscript, with contributions from all authors.

*A.A., J.B., and J.C. equally contributed to this work.

Corresponding author:

Correspondence to Jae-Kyung Lee (jamlee@uga.edu)

Acknowledgements: We thank Azucena Gomez-Cabrero and Jason Richardson's laboratory for expert technical assistance.

AUTHOR INFORMATION

Authors and Affiliations

Department of Physiology and Pharmacology, College of Veterinary Medicine, University of Georgia, Athens, GA, USA

Adetutu Adebowale, Jung Ha Byun, Jaegwon Chung, Hyun-Joon Lee, Declan Gresham, Jina Lim, Jae-Kyung Lee

Integrative Physiology and Pharmacology Program, University of Georgia, Athens, GA, USA.

Adetutu Adebowale, Declan Gresham, Jae-Kyung Lee

Neuroscience program, University of Georgia, Athens, GA, USA.

Jung Ha Byun, Jae-Kyung Lee

Additional information

NA

References

1. Kalia LV, Lang AE. Parkinson's disease. The Lancet. 2015;386(9996):896-912.
2. Spillantini MG, Crowther RA, Jakes R, Hasegawa M, Goedert M. α-Synuclein in filamentous inclusions of Lewy bodies from Parkinson's disease and dementia with Lewy bodies. Proceedings of the National Academy of Sciences. 1998;95(11):6469-73.
3. Sulzer D, Surmeier DJ. Neuronal vulnerability, pathogenesis, and Parkinson's disease. Movement Disorders. 2013;28(6):715-24.
4. Bloem BR, Okun MS, Klein C. Parkinson's disease. The Lancet. 2021;397(10291):2284-303.
5. Armstrong MJ, Okun MS. Diagnosis and treatment of Parkinson disease: a review. Jama. 2020;323(6):548-60.
6. Schapira AH, Chaudhuri KR, Jenner P. Non-motor features of Parkinson disease. Nature Reviews Neuroscience. 2017;18(7):435-50.
7. Reale M, Iarlori C, Thomas A, Gambi D, Perfetti B, Di Nicola M, Onofrj M. Peripheral cytokines profile in Parkinson's disease. Brain, behavior, and immunity. 2009;23(1):55-63.
8. Williams-Gray C. Wijeyekoon R1, Yarnall AJ2, Lawson RA2, Breen DP1, Evans JR1, Cummins GA1, Duncan GW3, Khoo TK4, Burn DJ2, Barker RA1; ICICLE-PD study group. Serum immune markers and

disease progression in an incident Parkinson's disease cohort (ICICLE-PD). Mov Disord. 2016;31(7):995-1003.

9. Béraud D, Hathaway HA, Trecki J, Chasovskikh S, Johnson DA, Johnson JA, et al. Microglial activation and antioxidant responses induced by the Parkinson's disease protein α-synuclein. Journal of Neuroimmune Pharmacology. 2013;8:94-117.
10. Baba Y, Kuroiwa A, Uitti RJ, Wszolek ZK, Yamada T. Alterations of T-lymphocyte populations in Parkinson disease. Parkinsonism & related disorders. 2005;11(8):493-8.
11. Williams GP, Schonhoff AM, Jurkuvenaite A, Gallups NJ, Standaert DG, Harms AS. CD4 T cells mediate brain inflammation and neurodegeneration in a mouse model of Parkinson's disease. Brain. 2021;144(7):2047-59.
12. Scott KM, Chong YT, Park S, Wijeyekoon RS, Hayat S, Mathews RJ, et al. B lymphocyte responses in Parkinson's disease and their possible significance in disease progression. Brain Communications. 2023;5(2):fcad060.
13. Poli A, Kmiecik J, Domingues O, Hentges F, Blery M, Chekenya M, et al. NK cells in central nervous system disorders. J Immunol. 2013;190(11):5355-62.
14. Small CL, McCormick S, Gill N, Kugathasan K, Santosuosso M, Donaldson N, et al. NK cells play a critical protective role in host defense against acute extracellular Staphylococcus aureus bacterial infection in the lung. J Immunol. 2008;180(8):5558-68.
15. Schmidt RL, Filak HC, Lemon JD, Potter TA, Lenz LL. A LysM and SH3-domain containing region of the Listeria monocytogenes p60 protein stimulates accessory cells to promote activation of host NK cells. PLoS Pathog. 2011;7(11):e1002368.
16. Sagiv A, Biran A, Yon M, Simon J, Lowe SW, Krizhanovsky V. Granule exocytosis mediates immune surveillance of senescent cells. Oncogene. 2013;32(15):1971-7.
17. Thoren FB, Riise RE, Ousback J, Della Chiesa M, Alsterholm M, Marcenaro E, et al. Human NK Cells induce neutrophil apoptosis via an NKp46- and Fas-dependent mechanism. J Immunol. 2012;188(4):1668-74.
18. Waggoner SN, Kumar V. Evolving role of 2B4/CD244 in T and NK cell responses during virus infection. Front Immunol. 2012;3:377.
19. Martin-Fontecha A, Thomsen LL, Brett S, Gerard C, Lipp M, Lanzavecchia A, Sallusto F. Induced recruitment of NK cells to lymph nodes provides IFN-gamma for T(H)1 priming. Nat Immunol. 2004;5(12):1260-5.
20. Vitale M, Della Chiesa M, Carlomagno S, Pende D, Arico M, Moretta L, Moretta A. NK-dependent DC maturation is mediated by TNFalpha and IFNgamma released upon engagement of the NKp30 triggering receptor. Blood. 2005;106(2):566-71.
21. Li Q, Cheng Z, Zhou L, Darmanis S, Neff NF, Okamoto J, et al. Developmental Heterogeneity of Microglia and Brain Myeloid Cells Revealed by Deep Single-Cell RNA Sequencing. Neuron. 2019;101(2):207-23 e10.

22. Van Hove H, Martens L, Scheyltjens I, De Vlaminck K, Pombo Antunes AR, De Prijck S, et al. A single-cell atlas of mouse brain macrophages reveals unique transcriptional identities shaped by ontogeny and tissue environment. Nat Neurosci. 2019.
23. Mihara T, Nakashima M, Kuroiwa A, Akitake Y, Ono K, Hosokawa M, et al. Natural killer cells of Parkinson's disease patients are set up for activation: a possible role for innate immunity in the pathogenesis of this disease. Parkinsonism Relat Disord. 2008;14(1):46-51.
24. Niwa F, Kuriyama N, Nakagawa M, Imanishi J. Effects of peripheral lymphocyte subpopulations and the clinical correlation with Parkinson's disease. Geriatr Gerontol Int. 2012;12(1):102-7.
25. Chen L, Zuo Y, Zhu L, Zhang Y, Li S, Ma F, et al. Peripheral venous blood neutrophil-to-lymphocyte ratio predicts survival in patients with advanced gastric cancer treated with neoadjuvant chemotherapy. Onco Targets Ther. 2017;10:2569-80.
26. Earls RH, Menees KB, Chung J, Barber J, Gutekunst CA, Hazim MG, Lee JK. Intrastriatal injection of preformed alpha-synuclein fibrils alters central and peripheral immune cell profiles in non-transgenic mice. J Neuroinflammation. 2019;16(1):250.
27. Earls RH, Menees KB, Chung J, Gutekunst CA, Lee HJ, Hazim MG, et al. NK cells clear alpha-synuclein and the depletion of NK cells exacerbates synuclein pathology in a mouse model of alpha-synucleinopathy. Proc Natl Acad Sci U S A. 2020;117(3):1762-71.
28. Earls RH, Menees KB, Chung J, Gutekunst C-A, Lee HJ, Hazim MG, et al. NK cells clear α-synuclein and the depletion of NK cells exacerbates synuclein pathology in a mouse model of α-synucleinopathy. Proceedings of the National Academy of Sciences. 2020;117(3):1762-71.
29. Giasson BI, Murray IV, Trojanowski JQ, Lee VM. A hydrophobic stretch of 12 amino acid residues in the middle of alpha-synuclein is essential for filament assembly. J Biol Chem. 2001;276(4):2380-6.
30. Rutherford NJ, Sacino AN, Brooks M, Ceballos-Diaz C, Ladd TB, Howard JK, et al. Studies of lipopolysaccharide effects on the induction of alpha-synuclein pathology by exogenous fibrils in transgenic mice. Mol Neurodegener. 2015;10:32.
31. Lei P, Ayton S, Moon S, Zhang Q, Volitakis I, Finkelstein DI, Bush AI. Motor and cognitive deficits in aged tau knockout mice in two background strains. Molecular neurodegeneration. 2014;9:1-12.
32. Lee JK, Tansey MG. Microglia isolation from adult mouse brain. Methods Mol Biol. 2013;1041:17-23.
33. Lee JK, Chung J, Kannarkat GT, Tansey MG. Critical role of regulator G-protein signaling 10 (RGS10) in modulating macrophage M1/M2 activation. PLoS One. 2013;8(11):e81785.
34. Zhang Y, Wallace DL, de Lara CM, Ghattas H, Asquith B, Worth A, et al. In vivo kinetics of human natural killer cells: the effects of ageing and acute and chronic viral infection. Immunology. 2007;121(2):258-65.
35. Prlic M, Blazar BR, Farrar MA, Jameson SC. In vivo survival and homeostatic proliferation of natural killer cells. J Exp Med. 2003;197(8):967-76.
36. Wang JW, Howson JM, Ghansah T, Desponts C, Ninos JM, May SL, et al. Influence of SHIP on the NK repertoire and allogeneic bone marrow transplantation. Science. 2002;295(5562):2094-7.

37. Ohira M, Ohdan H, Mitsuta H, Ishiyama K, Tanaka Y, Igarashi Y, Asahara T. Adoptive transfer of TRAIL-expressing natural killer cells prevents recurrence of hepatocellular carcinoma after partial hepatectomy. Transplantation. 2006;82(12):1712-9.
38. Earls RH, Lee JK. The role of natural killer cells in Parkinson's disease. Exp Mol Med. 2020;52(9):1517-25.
39. Carapito R, Bahram S. Genetics, genomics, and evolutionary biology of NKG2D ligands. Immunol Rev. 2015;267(1):88-116.
40. Vance RE, Kraft JR, Altman JD, Jensen PE, Raulet DH. Mouse CD94/NKG2A is a natural killer cell receptor for the nonclassical major histocompatibility complex (MHC) class I molecule Qa-1(b). J Exp Med. 1998;188(10):1841-8.
41. Mamula D, Khosousi S, He Y, Lazarevic V, Svenningsson P. Impaired migratory phenotype of CD4(+) T cells in Parkinson's disease. NPJ Parkinsons Dis. 2022;8(1):171.
42. Scott KM, Chong YT, Park S, Wijeyekoon RS, Hayat S, Mathews RJ, et al. B lymphocyte responses in Parkinson's disease and their possible significance in disease progression. Brain Commun. 2023;5(2):fcad060.
43. Santos-Lima B, Pietronigro EC, Terrabuio E, Zenaro E, Constantin G. The role of neutrophils in the dysfunction of central nervous system barriers. Front Aging Neurosci. 2022;14:965169.
44. Hosseini S, Shafiabadi N, Khanzadeh M, Ghaedi A, Ghorbanzadeh R, Azarhomayoun A, et al. Neutrophil to lymphocyte ratio in parkinson's disease: a systematic review and meta-analysis. BMC Neurol. 2023;23(1):333.
45. Keren-Shaul H, Spinrad A, Weiner A, Matcovitch-Natan O, Dvir-Szternfeld R, Ulland TK, et al. A Unique Microglia Type Associated with Restricting Development of Alzheimer's Disease. Cell. 2017;169(7):1276-90 e17.
46. Lu L, Ikizawa K, Hu D, Werneck MB, Wucherpfennig KW, Cantor H. Regulation of activated CD4+ T cells by NK cells via the Qa-1-NKG2A inhibitory pathway. Immunity. 2007;26(5):593-604.
47. Leavenworth JW, Schellack C, Kim HJ, Lu L, Spee P, Cantor H. Analysis of the cellular mechanism underlying inhibition of EAE after treatment with anti-NKG2A F(ab')2. Proc Natl Acad Sci U S A. 2010;107(6):2562-7.
48. Backstrom E, Chambers BJ, Kristensson K, Ljunggren HG. Direct NK cell-mediated lysis of syngenic dorsal root ganglia neurons in vitro. J Immunol. 2000;165(9):4895-900.
49. Davies AJ, Kim HW, Gonzalez-Cano R, Choi J, Back SK, Roh SE, et al. Natural Killer Cells Degenerate Intact Sensory Afferents following Nerve Injury. Cell. 2019;176(4):716-28 e18.
50. Verma DK, Seo BA, Ghosh A, Ma SX, Hernandez-Quijada K, Andersen JK, et al. Alpha-Synuclein Preformed Fibrils Induce Cellular Senescence in Parkinson's Disease Models. Cells. 2021;10(7).

Figures

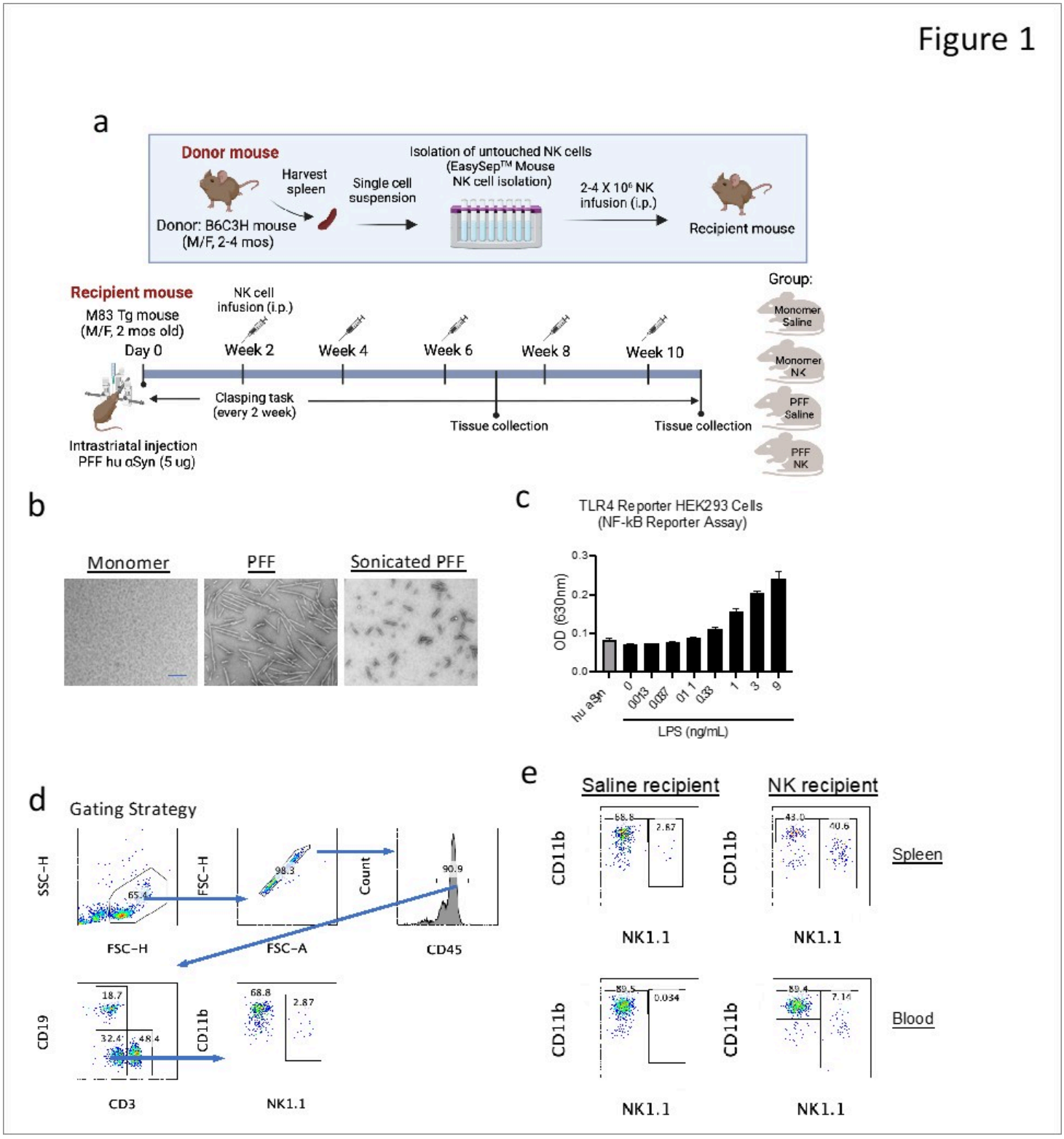


Figure 1

Systemic NK infusion leads to significant increases of NK cells in the spleen and blood of recipient mice. **(a)**Schematic of NK Cell Transfer Experimental Design. Untouched NK cells were isolated from the spleens of background-matched B6C3H donor mice (male and female, 2–4 mos old) using negative selection (EasySep™ Mouse NK Cell Isolation Kit). Single-cell suspensions of enriched NK cells (2 or 4 × 10^6 cells) were administered intraperitoneally (i.p.) into recipient M83 Tg mice (homozygous, male and

female, 2-mos old) that had been stereotaxically injected with 5 µg of human aSyn PFF or monomer into the striatum. NK cell infusions were performed biweekly, starting at 2 weeks post-injection. Motor function was assessed using the hindlimb clasping task every two weeks. Tissues were collected at 7- and 11-weeks post-injection to evaluate aSyn pathology, neurodegeneration, and immune responses. **(b)** Representative images of aSyn monomers, PFF, and sonicated PFF under TEM microscopy. Scale bar = 100 nm. **(c)** TLR4 reporter assay using HEK293 cells demonstrates dose-dependent activation of NF-κB signaling by lipopolysaccharide (LPS), with human aSyn (hu aSyn) alone showing minimal activation. **(d)** Gating strategy for flow cytometry. **(e)** Flow cytometry analysis of NK cells in spleen and blood samples from recipient mice were performed 3 days after i.p. injection.

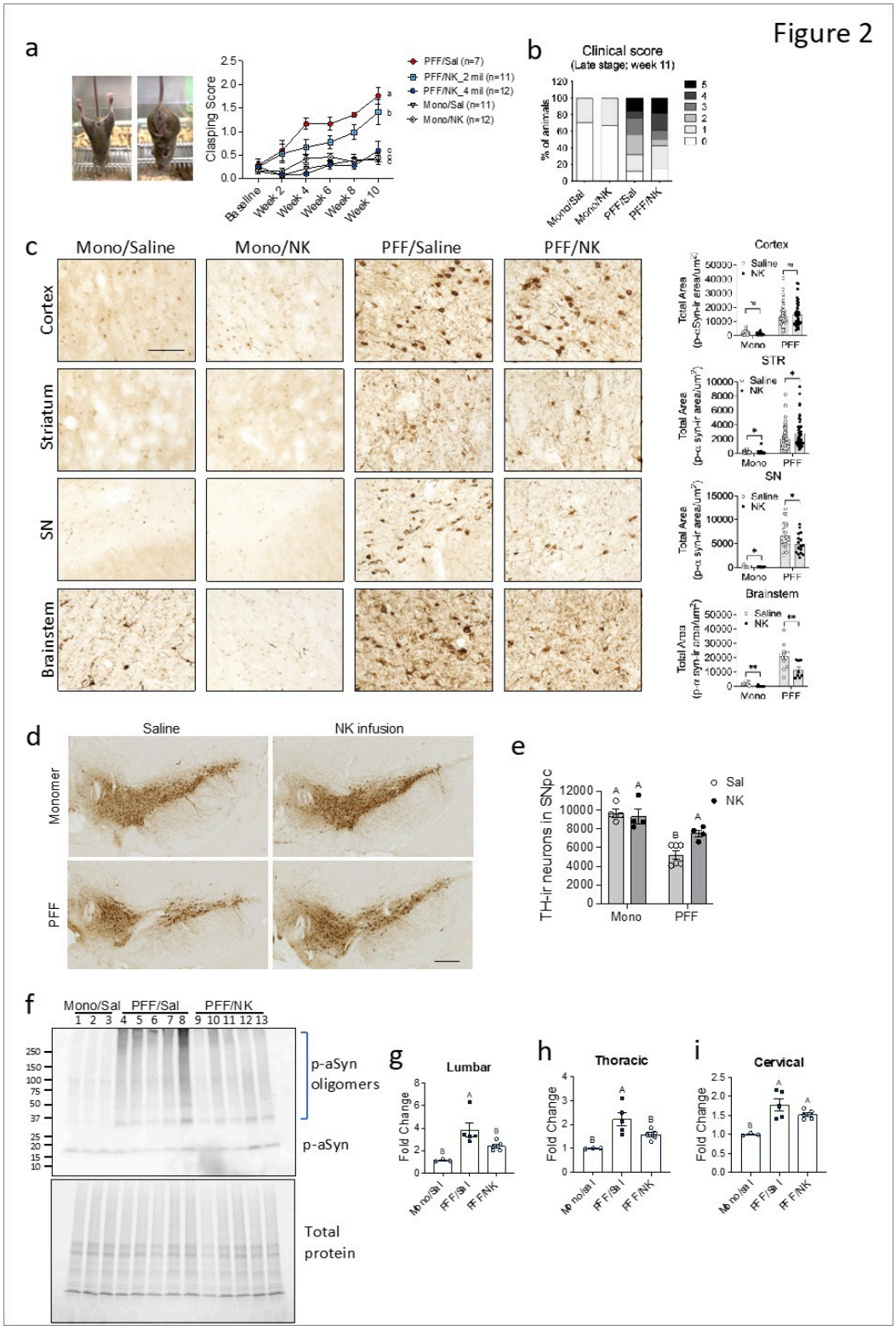


Figure 2

NK cell transfer ameliorates motor deficits, aSyn burden and neurodegeneration in the aSyn PFF M83 mouse model. (a) Representative images show clasping scores of 0 (left) and 3 (right). Graph shows quantitative clasping scores over time. Data were analyzed using two-way ANOVA followed by Tukey's post hoc test (n = 7–12 mice/group). Error bars represent mean ± SEM. Different letters indicate statistically significant group differences. **(b)** Clinical symptoms were assessed at 11 weeks post-

injection, as described in the Methods. **(c)** Representative images of PK-resistant p-aSyn pathology in the cortex, striatum, SN, and brainstem at 11 weeks post-injection (n = 4–6 mice/group). Mice received either monomeric or PFF aSyn and were treated with saline or NK cells. Scale bar = 100 μm. Graphs show quantification of total PK-resistant p-aSyn+ area per region of interest. Two-way ANOVA with Fisher's LSD post hoc test, *p < 0.05, **p < 0.001. Error bars represent mean ± SEM. **(d)** Representative images of TH-positive neurons in the SNpc. Scale bar = 500 μm. **(e)** Quantification of TH-positive neurons using unbiased stereological analysis. Data analyzed by two-way ANOVA with Fisher's LSD post hoc test. Different letters indicate statistically significant group differences. Error bars represent mean ± SEM. **(f)** Quantitative analysis of p-aSyn levels in spinal cord (lumbar region) of M83 Tg mice injected with PFF aSyn group and mono aSyn saline group at 7 weeks post-injection (n = 3 to 5 mice per group). Mice were treated with either saline or 4 million NK cells (i.p) every 2 weeks. The graph represents the quantification of p-aSyn levels in lumbar (g), thoracic (h) and cervical spinal cord (i). Data were analyzed using one-way ANOVA. Different letters (A, B) indicate statistically significant differences between groups ($p<0.05$).

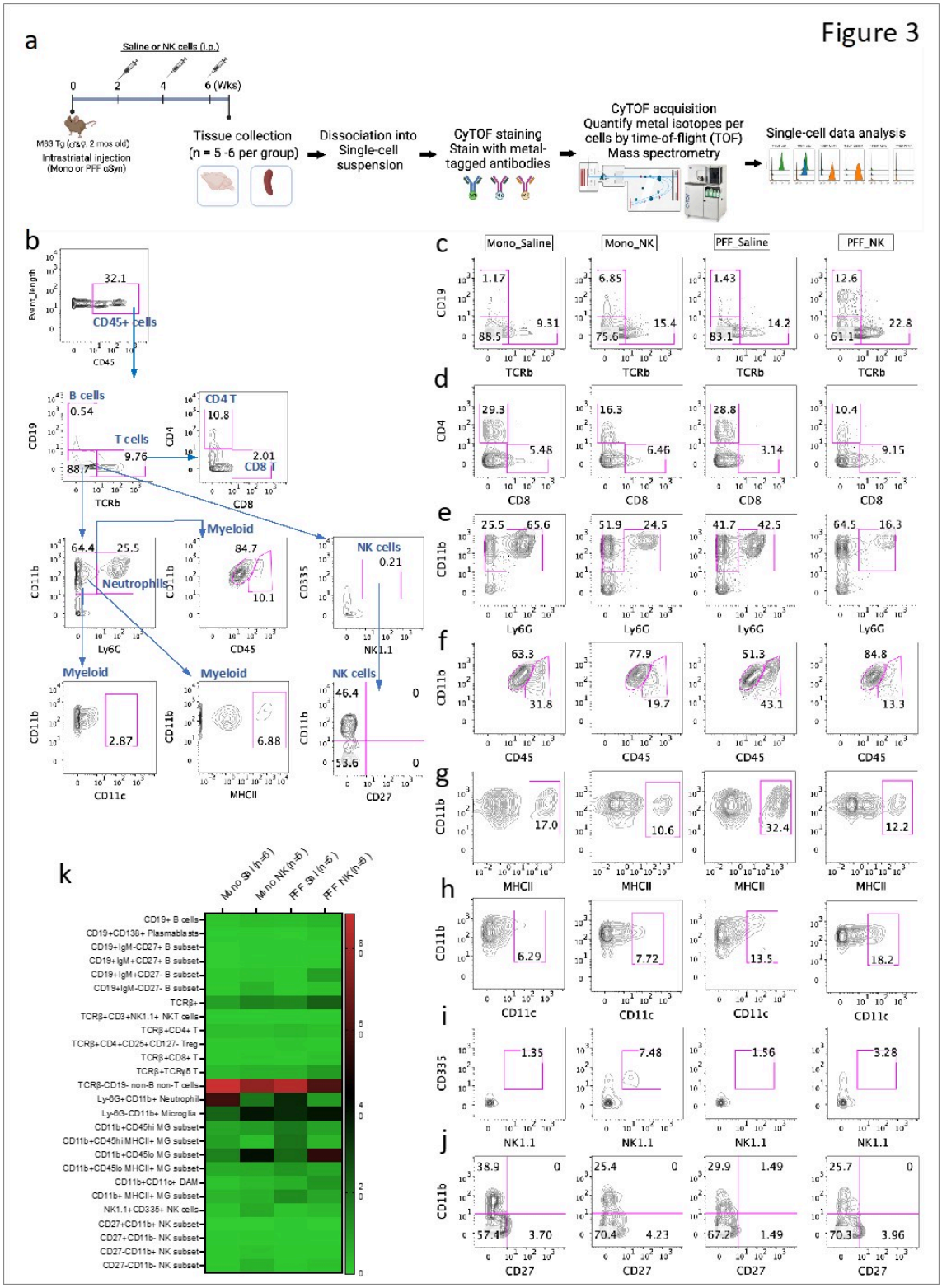


Figure 3

NK cell transfer reduces neuroinflammation and peripheral cell infiltration in the CNS in the a-Syn PFF M83 mice. (a) Schematic of the experimental workflow. M83 mice received unilateral intrastriatal injections of monomeric or aSyn PFF and were treated biweekly with saline or NK cells. At 7 weeks post-injection, mice were perfused with PBS to remove circulating blood cells, brains were harvested, processed into single-cell suspensions, pooled, stained with metal-tagged antibodies, and analyzed by

CyTOF mass cytometry. **(b)** Gating strategy for identification of major immune cell populations, including CD45⁺ leukocytes, B cells, T cells (CD4⁺, CD8⁺), myeloid cells and NK cells in saline injected non-surgical baseline control mice (pooled, n=5). **(c–j)** Representative contour plots showing frequencies of immune subsets across treatment groups (*n* = 5–6 mice per group): B cells (c), T cells (d), neutrophils (e), myeloid cells (f, g, h), and NK cells (i, j). Experimental groups include Mono/Saline, Mono/NK, PFF/Saline, and PFF/NK. **(k)** Heatmap summarizing the relative abundance of immune cell subsets in each group.

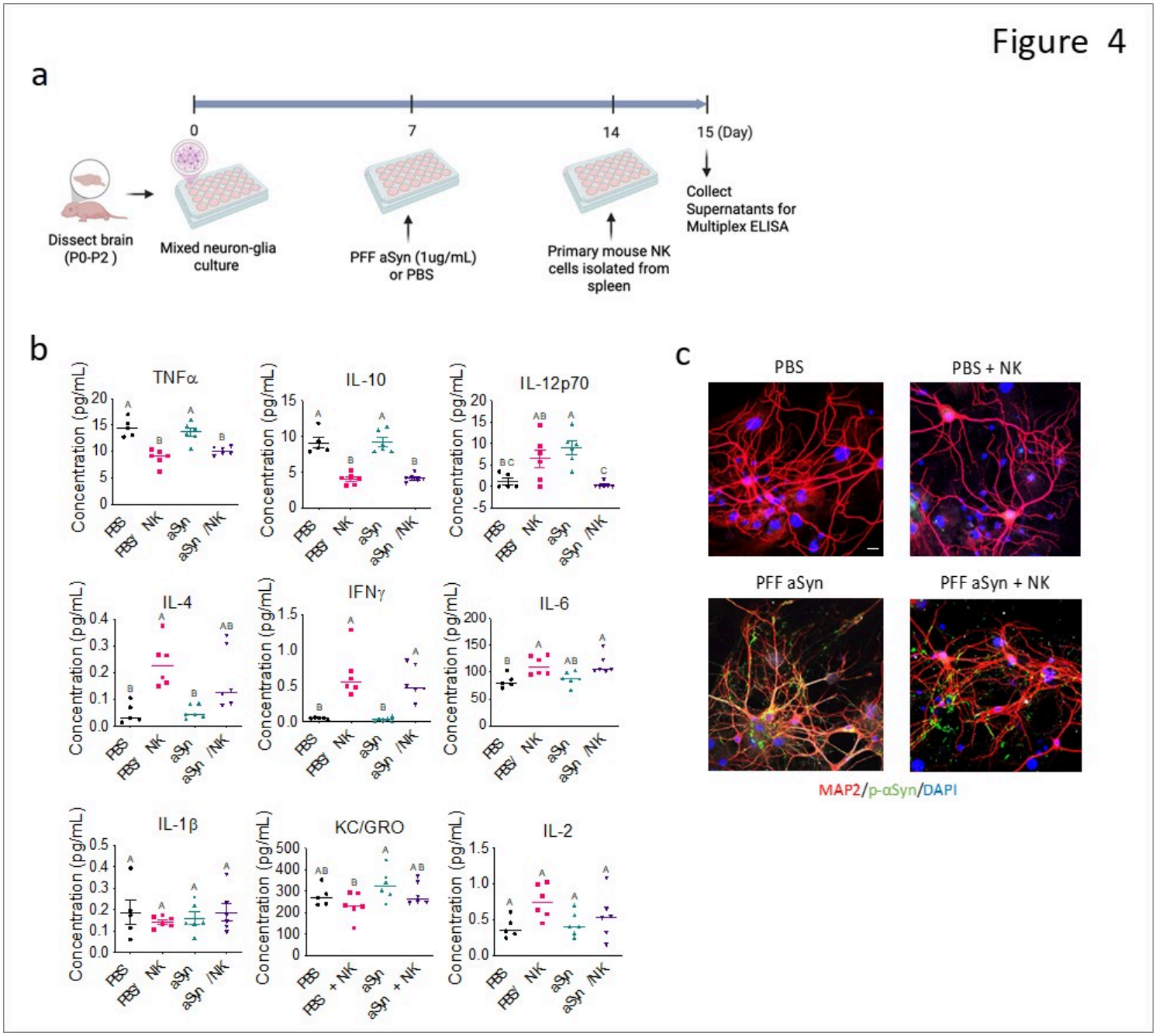


Figure 4

NK cells directly modulate neuroinflammatory responses in aSyn-challenged primary neuron-glia cultures. (a) Schematic of the mixed neuron-glia and NK cell co-culture experiment. Brains from postnatal day 0–2 (P0–P2) mice were dissected to establish mixed neuron-glia cultures. On Day 7,

cultures were treated with either sonicated aSyn PFF (1 μg/mL) or PBS. On Day 14, NK cells isolated from mouse spleens were added to the cultures. Supernatants were collected on Day 15 for multiplex ELISA analysis of cytokine and chemokine profiles. **(b)** Quantification of cytokine levels (pg/mL) for TNFα, IL-10, IL-12p70, IL-4, IFNγ, IL-6, IL-1β, KC/GRO, and IL-2 across four experimental conditions. Data are presented as individual values with mean ± SEM. Statistical analysis was performed using one-way ANOVA with Tukey's post hoc test. Groups labeled with different letters (A, B, C) are statistically different at $p < 0.05$. **(c)** Representative immunofluorescence images of neuron-glia cultures under the different treatment conditions. Red: neuronal marker; Green: glial marker; Blue: nuclear stain (DAPI). Scale bar: 50 μm.

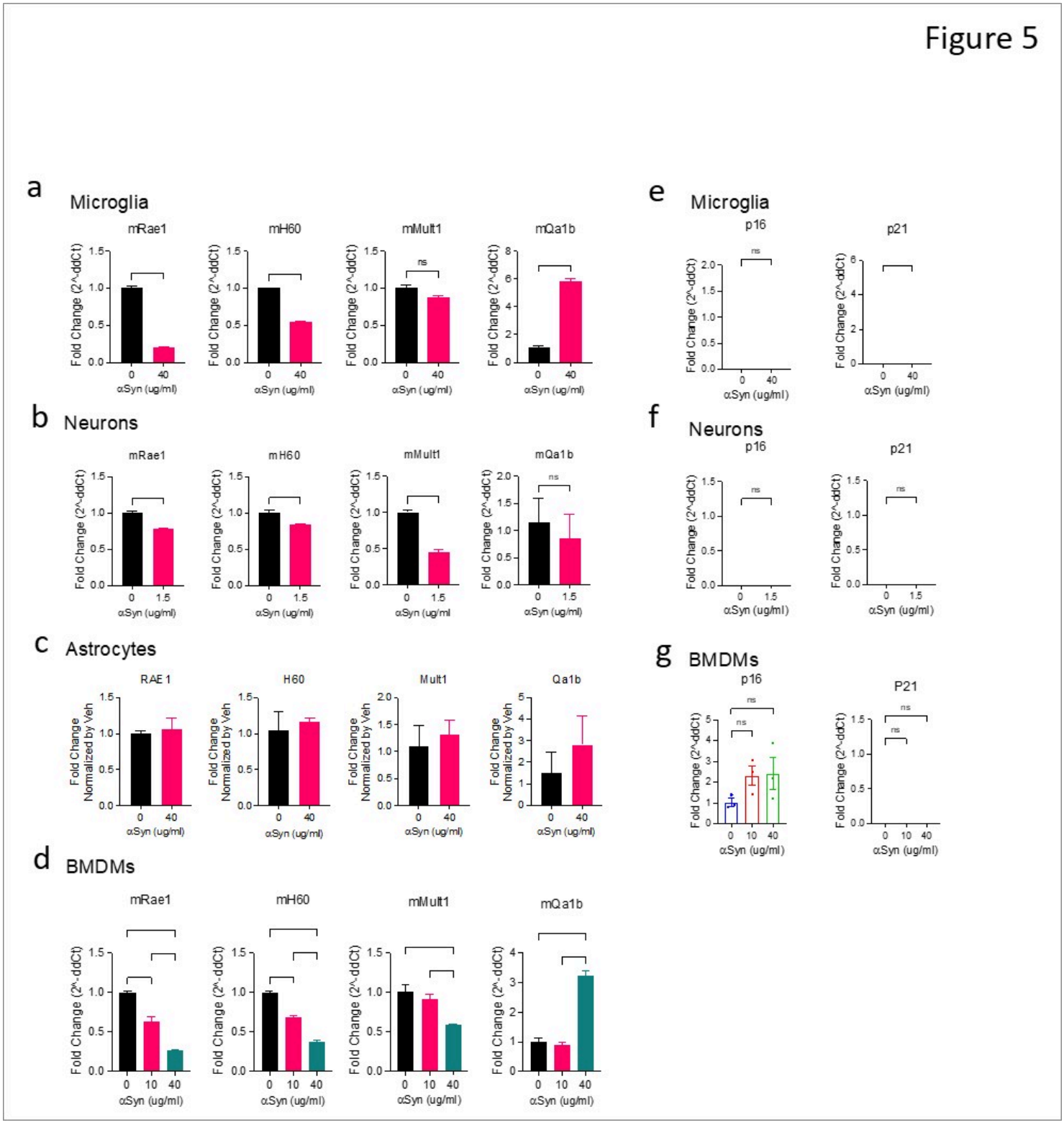


Figure 5

aSyn alters NK cell ligand expression and induces senescence-associated profiles in neural and myeloid cells. (a-d) Quantitative analyses of mRNA levels of NK receptor ligands (mRae1, mH60, mMult1, and mQa1b) in primary microglia (a), neurons (b), astrocytes (c), and BMDM (d) following aSyn treatment. Microglia, astrocytes, and BMDMs were treated with 0, 10, or 40 µg/mL aSyn, while neurons were treated with 0 or 1.5 µg/mL due to their higher sensitivity. Data are presented as fold change ($2^{-\Delta\Delta Ct}$) relative to

untreated controls. **(e-g)** Expression of senescence markers p16 and p21 in microglia (e), neurons (f), and BMDMs (g) after aSyn exposure. Data are presented as individual values with mean ± SEM. Statistical analyses were performed using Student's t-test or one-way ANOVA with Tukey's post hoc test. *p < 0.05, **p < 0.01, ***p < 0.001, ****p < 0.0001.

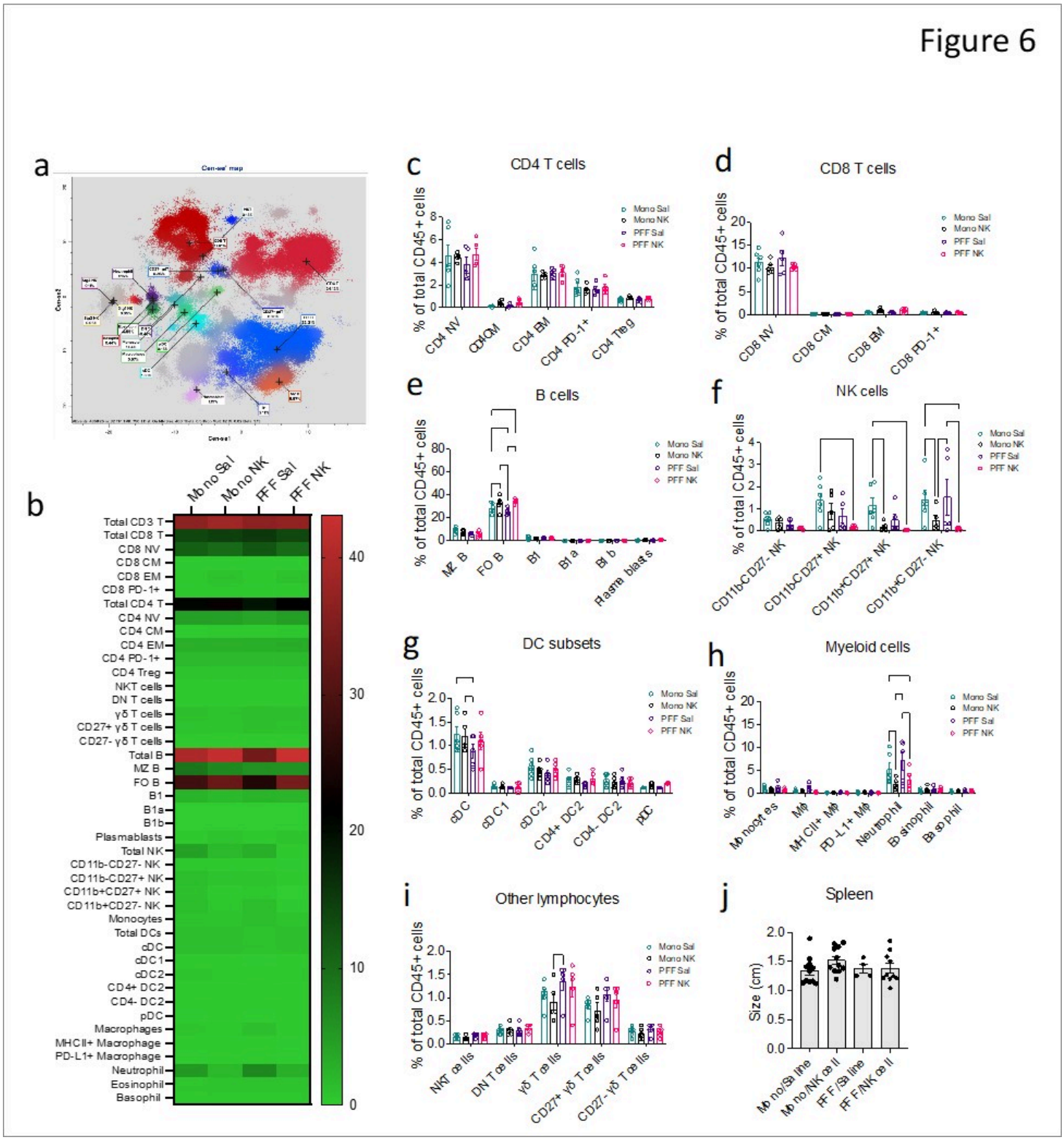


Figure 6

Systemic NK cell transfer modulates peripheral immunity by increasing follicular B cells and reducing neutrophils. M83 transgenic mice received unilateral intrastriatal injections of either monomeric aSyn or aSyn PFF and were treated biweekly with saline or NK cells. At 7 weeks post-injection, mice were perfused with PBS; spleens were harvested, processed into single-cell suspensions, pooled, stained with metal-tagged antibodies, and analyzed by CyTOF mass cytometry. **(a)** Cen-se' dimensional reduction map showing clustering of major splenic immune cell populations. **(b)** Heatmap of relative frequencies (%) of immune subsets across experimental groups; color intensity reflects subset percentage (scale 0–40%). **(c–d)** Frequencies of $CD4^+$ T cell (c) and $CD8^+$ T cell (d) subsets among total $CD45^+$ cells, including naïve (NV), central memory (CM), effector memory (EM), $PD\text{-}1^+$, and regulatory T cells (Tregs, $CD4^+$ only). **(e)** B cell subset analysis showing significant expansion of MZ and FO B cells in NK-treated groups. **(f)** Frequencies of NK cell subsets based on CD11b and CD27 expression, confirming NK cell expansion in treated groups. **(g)** DC subset composition, including conventional DCs (cDC, cDC1, cDC2), $CD4^+$ and $CD4^-$ DC2s, and plasmacytoid DCs (pDCs). **(h)** Frequencies of myeloid cell populations showing significant reduction in $MHCII^+$ macrophages in PFF/NK compared to PFF/Sal groups. **(i)** Other lymphocyte populations, including NKT cells, double-negative (DN) T cells, and γδ T cells. **(j)** Spleen size (cm) showing no significant differences across groups. Data are presented as mean ± SEM (n = 5–6 mice per group). Statistical significance was determined by one-way ANOVA with Tukey's post hoc test. *p < 0.05, **p < 0.01, ***p < 0.001, ****p < 0.0001.

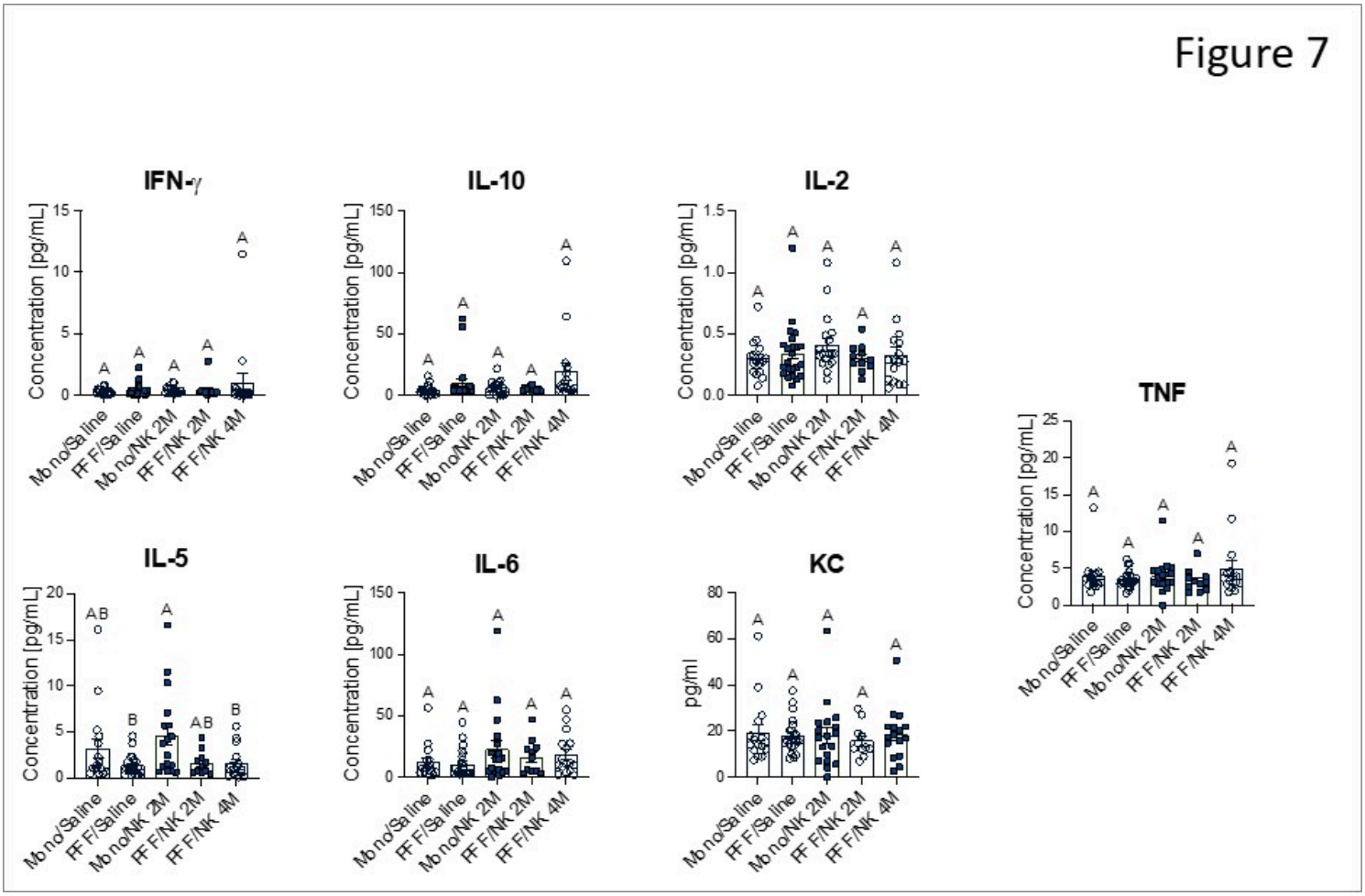


Figure 7

NK cell infusion does not alter systemic cytokine profiles. Serum samples were collected from mice at 11 weeks post-treatment and assessed for cytokine levels using multiplex assays. Experimental groups included monomeric aSyn with saline (Mono/Sal), PFF aSyn with saline (PFF/Sal), monomeric aSyn with NK cell infusion (Mono/NK), and PFF aSyn with NK cell infusion (PFF/NK). Untreated controls are shown for reference. Cytokine concentrations (pg/mL) are plotted for each mouse (each dot represents an individual sample). Data were analyzed using one-way ANOVA followed by Tukey's post hoc test. Groups labeled with different letters indicate statistically significant differences ($p < 0.05$).

Supplementary Files

This is a list of supplementary files associated with this preprint. Click to download.

- MNmanuscript042925Supplementdata.docx